batteries

MDPI

Review

A Review: Carbon Additives in $LiMnPO_4$- and $LiCoO_2$-Based Cathode Composites for Lithium Ion Batteries

Nam Hee Kwon *, Divine Mouck-Makanda and Katharina M. Fromm

Department of Chemistry, University of Fribourg, Chemin du Musée 9, CH-1700 Fribourg, Switzerland; divine.mouck-makanda@unifr.ch (D.M.-M.); katharina.fromm@unifr.ch (K.M.F.)

* Correspondence: namhee.kwon@unifr.ch; Tel.: +41-26-300-8735; Fax: +41-26-300-9738

Received: 16 September 2018; Accepted: 10 October 2018; Published: 15 October 2018

check for updates

Abstract: Carbon plays a critical role in improving the electronic conductivity of cathodes in lithium ion batteries. Particularly, the characteristics of carbon and its composite with electrode material strongly affect battery properties, governed by electron as well as Li^+ ion transport. We have reviewed here various types of carbon materials and organic carbon sources in the production of conductive composites of nano-$LiMnPO_4$ and $LiCoO_2$. Various processes of making these composites with carbon or organic carbon sources and their characterization have been reviewed. Finally, the type and amount of carbon and the preparation methods of composites are summarized along with their battery performances and cathode materials. Among the different processes of making a composite, ball milling provided the benefit of dense and homogeneous nanostructured composites, leading to higher tap-density and thus increasing the volumetric energy densities of cathodes.

Keywords: carbon; cathode composite; ball milling; energy density; lithium ion batteries

1. Introduction

Nowadays, lithium ion batteries are expanding their market and are used in electric vehicles and large energy storage systems. Large scale lithium ion batteries require higher energy density, longer lifetime and better safety compared to their small scale counterparts [1]. Lithium ion battery materials require both ionic and electronic conductivity for storing and providing electrical energy via redox electrochemical reactions during charge and discharge [2,3]. During charging, typically the active cathode material is oxidized at transition metal ions so as to release electrons and lithium ions. During discharging, the transition metal ion is reduced, based on the reverse reaction [4–6]. Because the active cathode material (LiM_xO_y, M = transition metals) is often lacking electronic conductivity, conductive carbon is added with the help of a binder (Figure 1) [7–16]. This carbon in a cathode does not involve the electrochemical reaction but solely supports the transport of electrons through the redox-active material. The microscopic structure of a cathode should furthermore be porous to allow a liquid electrolyte to penetrate inside, in order to ensure lithium ion transport (Figure 1 right). Hence, there is an electrolyte solid–liquid interface (marked in orange in Figure 1) where any solid surface is in contact with the liquid non-aqueous electrolyte [17]. The binder (grey in Figure 1) holds the particles together and provides a good adhesion to the current collector [18,19]. Among these components (redox material, carbon and binder) in the electrode, the composite made from the redox-active material and carbon is very important because it is directly related to the transport of electrons and lithium ions, responsible for the battery properties [20]. Carbon coating on the redox active material also protects the redox-active particles from dissolution of the transition metal ions into the electrolyte [15]. Therefore, prior to making a slurry with a binder and a solvent, the formation of composite is a crucial step to improve the cyclability and rate-capability of batteries [21–25].

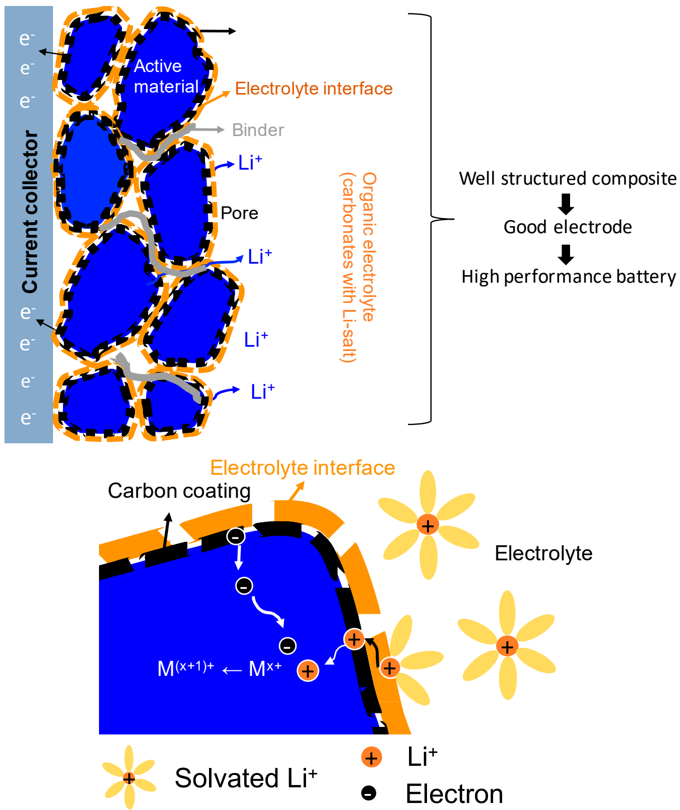

Figure 1. A schematic diagram of a cathode, consisting of an active material, carbon and a binder. The transport directions of electrons and lithium ions are shown as well.

The electronic conductivity of the composite varies depending on the composite structure, which itself depends on the preparation process and the type and morphology of both the carbon additive and the redox-active material. To obtain a sufficiently high electronic conductivity, the mixing homogeneity of carbon with the active material is one of the important parameters, which is also related to the preparation process to generate the electrode. The mixed composite can be prepared by various methods such as in-situ carbon coating via thermal heating [26–29], carbon deposition on the surface of active material via chemical vapor deposition (CVD) [28,30–34], mechanical milling [14,35–40] or hand/slurry mixing [10,41,42]. Another method of making a composite of carbon/redox active material is using a template to form a porous carbon network via thermal treatment [43,44]. Although using a template provides a 3D carbon network, improving the electronic conductivity of the composite, such highly porous carbon network reduces dramatically the volumetric energy density of lithium ion batteries because it leads to a low packing density of the redox active material.

This review focuses on efficient carbon coating methods in detail, physicochemical properties of the composites and battery performances of $LiMnPO_4$ and $LiCoO_2$ cathodes prepared by different mixing/coating methods.

2. Effect of Carbon Coating in $LiMnPO_4$ Electrodes on Battery Performance

Carbon coating on $LiMnPO_4$ particles provides two main advantages. The bare $LiMnPO_4$ has a relatively low electronic conductivity of 10^{-9}–10^{-13} S cm^{-1} [45–47] compared to other cathode materials, thus lowering capacity and rate-capabilities. Therefore, adding carbon improves the electronic conductivity of $LiMnPO_4$ electrode as shown in Figure 2a,b [15,48]. The electronic conductivity of C-$LiMnPO_4$ powder increased with the amount of acetylene carbon black until 30 wt% was above which no further improvement was observed (Figure 2a). Thus, such an amount of carbon-coated on $LiMnPO_4$ exhibited the best electrochemical properties, delivering 158 and 126 mAh g^{-1} of discharge capacities at C/20 and 1C, respectively [15]. Kumar et al. studied bare and carbon-coated $LiMnPO_4$ nanorods prepared by a modified polyol method and resin coating process. A resin was transformed to carbon after heating twice at 353 K and 623 K. They explained that carbon-coated $LiMnPO_4$ lowered the impedance compared to the pure one (Figure 2b). In the end, carbon-coated $LiMnPO_4$ exhibited 120–100 mAh g^{-1} at 1C, while the bare $LiMnPO_4$ nanorods exhibited 95–70 mAh g^{-1} at the same C-rate as shown in Figure 2c [48,49]. Barpanda et al. reported also that while pure $LiMnPO_4$ gave only 35 mAh g^{-1} of reversible capacity, sucrose and Ketjen black carbon-coated $LiMnPO_4$ delivered 95 mAh g^{-1} of discharge capacity at C/20 in CC (constant current) mode [50]. Figure 2d shows the morphology of C-$LiMnPO_4$ composite. High surface area, porous Ketjen black has been coated on the surface of $LiMnPO_4$ nanoparticles, enhancing charge transfer and lithium ion transport in the composite structure [14,15,36,51].

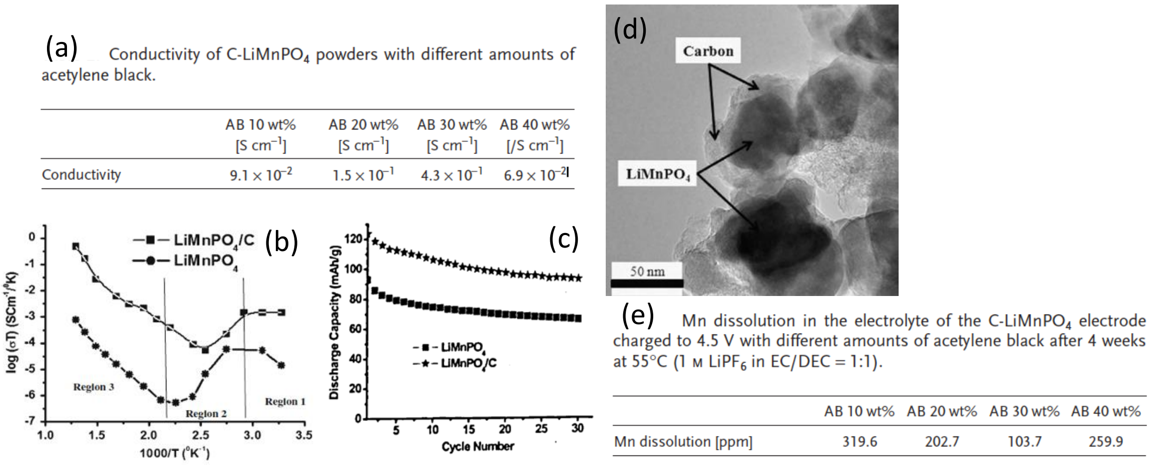
(a) Conductivity of C-$LiMnPO_4$ powders with different amounts of acetylene black.

	AB 10 wt% [S cm^{-1}]	AB 20 wt% [S cm^{-1}]	AB 30 wt% [S cm^{-1}]	AB 40 wt% [/S cm^{-1}]
Conductivity	9.1×10^{-2}	1.5×10^{-1}	4.3×10^{-1}	6.9×10^{-2}

(e) Mn dissolution in the electrolyte of the C-$LiMnPO_4$ electrode charged to 4.5 V with different amounts of acetylene black after 4 weeks at 55°C (1 M $LiPF_6$ in EC/DEC = 1:1).

	AB 10 wt%	AB 20 wt%	AB 30 wt%	AB 40 wt%
Mn dissolution [ppm]	319.6	202.7	103.7	259.9

Figure 2. (**a**) Conductivity of C-$LiMnPO_4$ composite powder with different amounts of acetylene black carbon [15]. (**b**) conductivities and (**c**) discharge capacities at 1C of bare and C-$LiMnPO_4$ nanorods [48]. (**d**) TEM image of $LiMnPO_4$ and Ketjen black carbon composite prepared by ball milling [14]. (**e**) Mn dissolution of the composite C-$LiMnPO_4$ electrode with different amounts of acetylene black carbon [15].

In order to obtain a high-performance of cathode, the Li^+ ion conductivity must be also high in combination with high electronic conductivity. The ionic conductivity of $LiMnPO_4$ can be enhanced by reducing the path length of Li^+ ions in a particle in which Li^+ ions are diffusing [52–55].

Another benefit of the carbon coating is to prevent the dissolution of manganese ions from $LiMnPO_4$ into the electrolyte. Oh et al. studied the manganese ion dissolution of the charged $LiMnPO_4$ electrode at 4.5 V with an amount of acetylene carbon black of 10 to 40 wt%. After four weeks at 55 °C in a commercial electrolyte, the dissolved amount of manganese ion with 30 wt% carbon was only 1/3 of that with 10 wt% of carbon as shown in Figure 2e. They explained that the homogeneous carbon coating protected the surface of $LiMnPO_4$ against HF attack, suppressing the dissolution of manganese as well as improving the electronic conductivity of the electrode [15]. Marth et al. reported that a $LiMnPO_4$/C composite was much less surface reactive with the organic electrolyte compared to transition metal oxide cathodes such as $LiCoO_2$, $LiNiO_2$, $LiMn_2O_4$, $Li(NiMnCo)O_2$ and $Li_xV_2O_5$. This low surface reactivity of $LiMnPO_4$/C has been attributed to both the uniform carbon coating and the low basicity of PO_4^{3-} [56].

The amount of conductive carbon is an important parameter, which is related to not only electron transfer but also loading of redox active material on a current collector. High amounts of carbon increase the electronic conductivity of the composite as mentioned [11,15,20] on one hand, but, on the other hand, decrease the energy density of $LiMnPO_4$ because of the lower amount of $LiMnPO_4$ in the composite [39,57,58]. This phenomenon is even more pronounced when both $LiMnPO_4$ and carbon particles are in the nanoscale because the packing density/tap density of nano-$LiMnPO_4$ with nano-carbon is low. The packing density also varies depending on the shape of nanoparticles of

$LiMnPO_4$. High aspect ratio particles such as needle-shaped ones have low tap density, while round or elongated-shaped nanoparticles have higher tap density [58]. Ni et al. calculated the gravimetric and volumetric capacities of 12 and 30 wt% of carbon containing electrodes. The packing density of $LiMnPO_4$ was 1.8 and 1.4 g cm^{-3} for the electrodes with 12 and 30 wt% carbon, respectively, and the corresponding volumetric capacity was 176 and 130 mAh cm^{-3} [39]. Aware of this aspect of decreased amount of active mass with increasing of carbon percentage in the electrode, Kwon et al. tested $LiMnPO_4$ electrodes with only 10 wt% of Ketjen black carbon obtained via ball milling. They provided the full capacity at C/20 when $LiMnPO_4$ is nano-rod-shaped and 20 × 30~100 nm in size. However, the rate capability was not satisfying at high current densities (>1C). The discharge capacity at 1C was 66 mAh g^{-1} with 10 wt% of Ketjen black carbon mixed with nano-$LiMnPO_4$ [59]. When the quantity of Ketjen black was increased to 30 wt%, the capacity of nano-$LiMnPO_4$ also increased to 80 mAh g^{-1} at the same current density of 1C [58]. Generating a dense agglomeration via ball milling and coprecipitation can increase the packing density/tap density of the composites [58,60]. Figure 3 shows the morphologies of composites C-$LiMnPO_4$, C-$LiFePO_4$ and C-$LiMn_{0.85}Fe_{0.15}PO_4$ prepared by ball milling (a) and coprecipitations (c) and (e), respectively. Their volumetric capacities are also shown in (b), (d) and (f), respectively. Increasing the packing densities of the C-$LiMnPO_4$ [58], C-$LiFePO_4$ [60] and C-$LiMn_{0.85}Fe_{0.15}PO_4$ [61] composites provided 3.5, 2.5 and 1.5 times higher volumetric capacities, respectively.

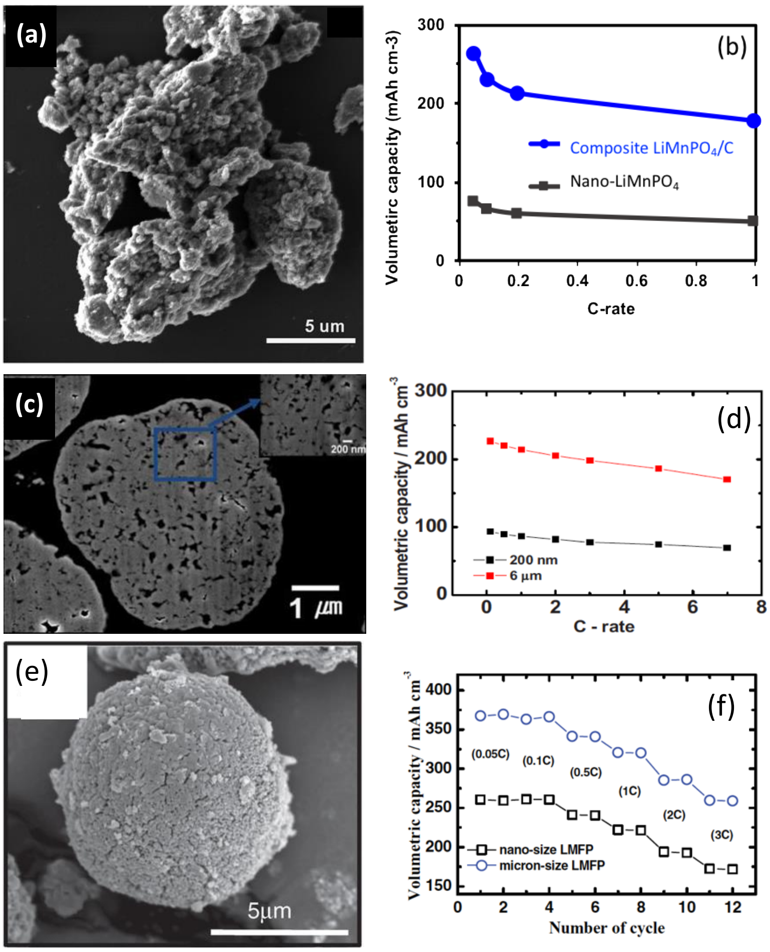

Figure 3. (**a**,**c**,**e**) The SEM images of Ketjen black carbon-$LiMnPO_4$ composite [58], carbon-$LiFePO_4$ [60] and carbon-$LiMn_{0.85}Fe_{0.15}PO_4$ [61], respectively. (**b**,**d**,**f**) Their volumetric capacities at various C-rates [58,60,61].

In summary, a carbon coating is essential to improve the electronic conductivity and specific capacities of $LiMnPO_4$ and to prevent transition metal ion dissolution in the electrolyte. However, as carbon is not electrochemically active in the cathode, the carbon amount should be minimized without decreasing the electronic conductivity in order to maximize the mass of redox-active cathode material in the electrode.

Yet, the electrode properties can vary not only depending on the types of carbonaceous materials or organic precursors, but also on the composite preparation process [39,49,62,63]. Two methods have been most widely studied for the preparation of the composite of $LiMnPO_4$ and carbon: (i) the thermal treatment of organic carbon precursors on $LiMnPO_4$ particles, and (ii) the mechanical milling of carbonaceous material and $LiMnPO_4$. The details of those two methods are reviewed in the next sections.

3. Organic Carbon Sources in the Composite of $LiMnPO_4$/C

In order to reduce the amount of carbon without sacrificing the electronic conductivity of the composite, organic carbon precursors have been considered to form a thin layer of carbon on the $LiMnPO_4$ particles. The reported carbon precursors are acrylic acid [48,49], L-ascorbic acid, sucrose [63,64], polyethylene oxide (PEO) and carboxymethyl cellulose (CMC) [65], cetyltrimethylammonium bromide (CTAB) [63], glucose [66], dextrose [67] and vapor grown carbon fibers (VGCF) [68]. Those have been dissolved in solution together with $LiMnPO_4$, then dried and thermal decomposition was carried out at temperature above 600 °C under an inert atmosphere. Zhao et al. prepared a $LiMnPO_4$/C composite by pyrolysis of sucrose. Sucrose was added in several steps while adding each of the $LiMnPO_4$ precursors sequentially. The pyrolysis was carried out at relatively low temperature of 550 °C for 2h in Ar atmosphere in order to suppress the grain growth during the thermal decomposition. This composite of $LiMnPO_4$/C achieved 142, 110, and 75 mAh g^{-1} at C/10, 1C and 5C, respectively [64]. Mizuno et al. studied four different types of organic carbon sources such as L-ascorbic acid, sucrose, polyethylene oxide (PEO) and CMC on $LiMnPO_4$. They were mixed with the precursor solution of $LiMnPO_4$ in an autoclave. The powder was collected, then carbon was created after thermal decomposition at 700 °C under 3% H_2/Ar flow. The structure and the amount of formed carbon varied depending on the carbon source. Thermal decomposition of the PEO sample did not show any carbon characteristic bands in Raman spectroscopy while the other carbon precursors were transformed to graphitic carbon as shown in Figure 4a. Thus, PEO was hardly coated on $LiMnPO_4$ while sucrose, CMC and ascorbic acid were transformed to 5.5 (the highest amount of carbon coating), 2.4 and 2.8 wt% of carbon coating, respectively. Although the highest amount of carbon coating on $LiMnPO_4$ was obtained with sucrose, the specific capacities of $LiMnPO_4$ with CMC showed the best performance as shown in Figure 4b, which was explained as CMC being converted to graphitic carbon more easily than other carbon sources. The authors mentioned that the presence of hydroxyl groups in the carbon precursor plays an important role in the formation of a carbon layer on the surface of the $LiMnPO_4$ particles [65].

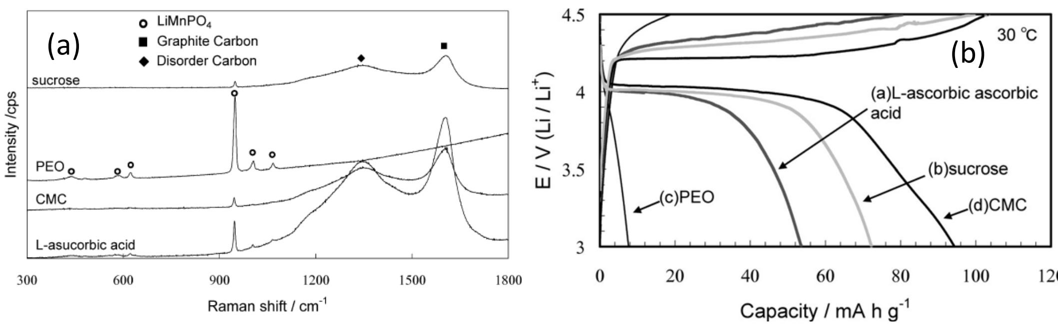

Figure 4. (**a**) Raman spectra of four different carbon sources used C-$LiMnPO_4$ composite. (**b**) Charge and discharge curves of $LiMnPO_4$ electrode prepared with various carbon sources [65].

Kim et al. studied carbon coatings formed with sucrose and cetyltrimethylammonium bromide (CTAB) after the precipitation of $LiMnPO_4$. They found no carbon content on $LiMnPO_4$ with CTAB as a carbon precursor after thermal treatment, while 8.5 wt% carbon was obtained with sucrose. They also reported that this coating behavior on $LiMnPO_4$ is different from that of $LiFePO_4$ and $LiMn_{0.5}Fe_{0.5}PO_4$, for which 2–4 wt% and 1.5 wt% of carbon were detected, respectively, using CTAB prepared by the same method as for $LiMnPO_4$ [63]. They claimed that this is due to the presence of Cr, Fe, Co, Ni and Cu that can act as catalysts for carbonization [69,70], while Mn is not catalytically active in this respect.

This thermal decomposition process can however lead e.g., to impurities due to the creation of a reducing environment [48,49], to partial carbon coating on the surface of $LiMnPO_4$ particles, and to the growth of the $LiMnPO_4$ particles due to the high temperature process [63,65,67]. The particle growth of $LiMnPO_4$ slows down the Li^+ diffusion kinetics because the Li^+ diffusion length increases as particles grow, hence lowering the specific capacity and rate capability. In this respect, the high temperature carbon coating method is not suitable to maintain a high Li^+ and e^- conductivity in the $LiMnPO_4$/C composites. Thus, several groups added extra carbon and mixed it into the composite by ball milling after preparing in-situ carbon coatings on $LiMnPO_4$ at high temperature [50,71,72].

Choi et al. prepared C-nanoplatelet $LiMnPO_4$ by using the molten hydrocarbon method and ball milling. The precursors of $LiMnPO_4$ were high-energy ball-milled (SPEX mill) with oleic acid and then further ball-milled with paraffin wax. After ball milling, the viscous slurry was heated to 550 °C for 8 h under 3% H_2/Ar atmosphere. This $LiMnPO_4$ was then planetary ball-milled with 25 wt% Ketjen black for 4 h. A discharge capacity of 54 mAh g^{-1} was delivered at 1C, but 117 mAh g^{-1} was attained at the same discharge rate after charging at C/25. This study showed that the practical discharge power density of $LiMnPO_4$ is close to that of $LiFePO_4$ when the charge rate is C/25 and the practical energy density of $LiMnPO_4$ (630 Wh kg^{-1}) is comparable to or even higher than that of $LiFePO_4$ at lower power (<30 W kg^{-1}) [71].

Bakenov et al. prepared C-$LiMnPO_4$ by spray pyrolysis and wet ball milling with 10 wt% acetylene black. The composite was fired then at 500 °C for 4 h in a N_2 + 3% H_2 atmosphere. The discharge capacities were 130 and 70 mAh g^{-1} at C/10 and 1C, respectively in a relatively higher voltage window between 2.5 and 4.9 V [72].

The thermal process with carbon and/or carbon precursors has two aims: one is to form carbon on the surface of $LiMnPO_4$ via thermal decomposition of organic precursors such as ascorbic acid, sucrose, polymers etc. [48,49,63,65,67,71]. The purpose of the second thermal treatment after ball milling is probably to recover the damaged carbon structure of carbonaceous materials. This treatment occurs between 500 and 600 °C under Ar or Ar/3% H_2 for 1–4 h and may improve the specific capacities [14,15,68,72–74].

In summary, using an organic precursor can create a thin and homogeneous carbon layer on the electrode materials. In this process, the type and amount of the organic source, the surface of active material and the annealing temperature should be considered. However, the electronic conductivity after the carbon coating via an organic precursor does not seem sufficiently increased.

4. Carbonaceous Materials in the Composite of $LiMnPO_4$/C

Another method to make a composite is to add the carbonaceous material directly to $LiMnPO_4$. In this case, several parameters should be considered to maximize the battery properties. Firstly, the amounts of carbon in a cathode should be kept to an as low as possible (depending on the morphology and the surface area of the active material) amount to achieve an ideal electrochemical reaction. Secondly, the physicochemical properties influence the structure of composite such as the morphology, electronic conductivity, surface area, powder density, packing density, defect density etc. [20,27]. Various carbonaceous materials have been studied to make a composite of carbon and $LiMnPO_4$: carbon black [14,15,36,37,39,50,65,71,73,75], carbon nanotubes (CNT) [76–81] and graphene [82–85]. Bakenov et al. studied three different types of nanosized carbon black in composites prepared by wet ball milling. Those carbonaceous materials were acetylene black with 68 m^2 g^{-1}

surface area and Ketjen black with two different surface areas of 800 and 1400 $m^2 g^{-1}$. Using the highest surface area of Ketjen black exhibited the highest surface area of the composite with $LiMnPO_4$. A large specific surface area can provide high ability to absorb the electrolyte, delivering an initial discharge capacity of 166 mAh g^{-1} at C/20. It then decreased rapidly to 100 mAh g^{-1} at 50th cycle with 20 wt% of Ketjen black. This may be influenced by a high upper potential of 4.9 V vs. Li^+/Li, causing a difficulty of Li^+ penetration into $LiMnPO_4$ particles due to a thick SEI layer. When the cut-off upper voltage was reduced to 4.4 V vs. Li^+/Li in constant current and constant voltage (CC-CV) mode, discharge capacity was decreased to 138 mAh g^{-1} at C/20 but higher C-rate capacities improved to 100 and 70 mAh g^{-1} at 1C and 5C, respectively [14]. Wang et al. prepared platelet-shaped thin $LiMnPO_4$ with 20 wt% of acetylene black by dry ball milling. The composite electrode exhibited a specific capacity of 145 and 113 mAh g^{-1} at C/20 and 1C, respectively. Thanks to the enhanced conductivities of Li^+ and e^- in the composite by reducing the Li^+ diffusion path length in a single particle and a homogeneous structure, the cut-off voltage was lowered to 4.4 V vs. Li^+/Li [37].

CNT as a conductive additive has been also applied in various electrode materials [76–81,86] as well as $LiMnPO_4$ electrodes [38,87,88]. Dettlaff-Weglikowska et al. reported that 1 wt% of single-walled carbon CNT (SWCNT) increased the electrical conductivity of $LiMnPO_4$ composite up to 5 orders of magnitude. However, the capacity of this composite cathode remained only 20 mAh g^{-1} at C/10, which is very low compared with other carbon containing $LiMnPO_4$ composite electrodes. CNT bucky paper as a self-supporting film combined with only 40 wt% of $LiMnPO_4$ provided an increased specific capacity of 125–148 mAh g^{-1} at C/10. However, the charge and discharge curves were rather sluggish instead of the typical plateau of $LiMnPO_4$ [38]. Vadivel Murugan et al. prepared olivine materials ($LiMPO_4$, M = Mn, Fe, Co and Ni) with multi-walled CNT (MWCNT) nanocomposites by magnetic stirring. Among four different olivine materials ($LiFePO_4$, $LiMnPO_4$, $LiCoPO_4$ and $LiNiPO_4$) with MWCNT, $LiMnPO_4$ showed the lowest rate capability as well as the largest particle size from the same synthesis [87], which hinders Li^+ diffusion. Kavan et al. prepared a solution of 1–10 wt% of MWCNT with $LiMnPO_4$ nanoparticles (SSA: 35 $m^2 g^{-1}$), $LiFePO_4$ (SSA: 9 $m^2 g^{-1}$) and TiO_2 as electrode materials. They reported that MWCNT with $LiMnPO_4$ showed an enhanced electrochemical charge/discharge performance but performed significantly lower with considerable irreversibility than MWCNT with $LiFePO_4$ under the same procedure. The specific capacity of $LiMnPO_4$ with 10 wt% of MWCNT exhibited only 72 mAh g^{-1} at C/10 while that of $LiFePO_4$ with the same amount of MWCNT reached 140 mAh g^{-1} even at 1C. They functionalized the surface of MWCNT by oxidation with HNO_3, which improved the reversibility of the $LiMnPO_4$ charge/discharge processes. However, the functional group of MWCNT mediated the parasitic breakdown reaction of organic electrolyte (EC:DMC, 1M $LiPF_6$) above 4.2 V, which is near the operating potential condition of $LiMnPO_4$ in Li-ion batteries [88]. Thus, although using CNT improved the electrical conductivity of $LiMnPO_4$ electrode with relatively a small amount compared to other carbonaceous materials, the capacity and rate capability of $LiMnPO_4$ did not improve as much as when using carbon black.

Graphene is also an attractive conductive additive because of the high in plane conductivity and it has high mechanical strength and structural stability [82–85,89,90]. The properties of graphene and its electrochemical behavior have been summarized and compared with other carbonaceous materials by Raccichini et al. [90] and Kucinskis et al. [89]. $LiMnPO_4$ electrodes with graphene have been prepared by many groups [40,91–93]. Zong et al. prepared a composite of $LiMnPO_4$ with graphene nanoplates by slurry and planetary milling using the sol-gel synthesis for $LiMnPO_4$ and chemically exfoliated graphene. They compared the impedance and the rate capability of this material with that of the acetylene black/$LiMnPO_4$ composite (Figure 5a,b). The capacities at low C-rates did not show much difference, but the composite of graphene/$LiMnPO_4$ provided superior rate capability at higher C-rates (0.5C and 1C) as shown in Figure 5b. They explained that 3D conducting network with graphene, small nanoparticles of $LiMnPO_4$, and reduced agglomeration of graphene/$LiMnPO_4$ provided the capacity of 139 and 119 mAh g^{-1} at 0.05 C and 1 C, respectively with the total amount of carbon of about 26 wt% in the electrode [40]. As another example with graphene, Wang et al. synthesized

$LiMn_{0.75}Fe_{0.25}PO_4$ nanorods on reduced graphene oxide (rGO) sheets. GO was reduced at the same time when the nanorods $LiMn_{0.75}Fe_{0.25}PO_4$ were formed on rGO sheets by the solvothermal method, shown in Figure 5c. The oxygen content of rGO was lower than that prepared by the Hummers method [94]. The combination of $LiMn_{0.75}Fe_{0.25}PO_4$ nanorods and rGO sheets yielded a superior rate capability of 153, 140 and 100 mAh g^{-1} at C/2, 10C (discharge in 6 min) and 100C (discharge in 36 s) as shown in Figure 5d,e [91]. Such a high rate capability was achieved under the condition of the fixed charging rate of C/20 with constant current -constant voltage. On the other hand, it has been also reported that the planar graphene sheets can block Li^+ mobility and decrease the battery performance [95–97].

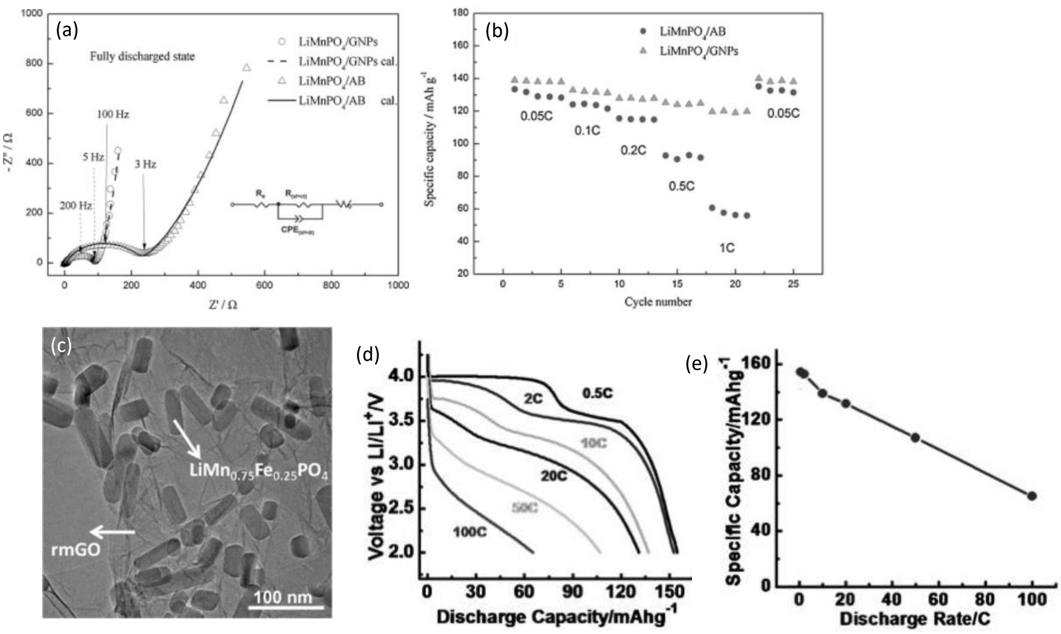

Figure 5. (**a**) AC impedance spectra and (**b**) rate capabilities of two composites $LiMnPO_4$ electrodes. AB is acetylene black and GNP is graphene nanoplates [40]. (**c**) TEM image of $LiMn_{0.75}Fe_{0.25}PO_4$ with graphene. (**d**) Discharge curves of $LiMn_{0.75}Fe_{0.25}PO_4$ nanorods on reduced graphene at various C-rates. (**e**) Specific capacities at different C-rates of $LiMn_{0.75}Fe_{0.25}PO_4$ and reduced graphene composite electrode [91].

In summary, a choice of carbonaceous material in a composite and a procedure of making a composite are very critical to reach the theoretical capacity of $LiMnPO_4$. In addition, the testing procedure is another parameter to maximize the specific capacities.

5. Ball Milling of Nanomaterials and $LiMnPO_4$/C Composite

This section focuses on the ball milling process to produce a composite because it is one of effective ways to generate a homogeneous mixture and mesoporous structure with nanoparticles. Ball milling or mechanical milling has several aims: reducing the particle size [98], mixing of powders [99–104] and synthesizing nanoparticles [105–107]. There are also several types of mechanical mills such as tumbler, vibration, planetary and attrition mills [108,109]. Depending on a type of ball milling, the energy and force (either shear or shock) vary and the degree of grinding or mixing varies as well [35,108,110,111]. The milling of nanomaterials rather forms agglomerations instead of breaking single particles, reducing the surface area of nanoparticles [39]. The size and volume of pores are reduced, and those agglomerated micron sized particles become denser upon milling. The milling time should be optimized [112] in order to avoid any side effects. A prolonged milling time may deform the surface and shape of the particles, and create an amorphous phase [111,113,114]. It can also deform the structure of materials [35,114] and set free iron ions, ZrO_2, and/or Al_2O_3 contaminations from the milling balls by a rupture of the balls themselves and grinding of the balls instead of materials [115–117].

Ni et al. reported the effect of ball milling on $LiMnPO_4$. They prepared $LiMnPO_4$ with sucrose as a carbon source at two heating steps of 300 and 650 °C for 2 and 5 h respectively under Ar flow. Then the $LiMnPO_4$ was furthered high-energy ball-milled and high-speed planetary milled with 8 wt% of acetylene black. This ball-milled $LiMnPO_4$/C delivered capacities in the range of 120–130 and 96–100 mAh g^{-1} at C/10 and 1C, respectively at 30 °C while the non-ball-milled $LiMnPO_4$ delivered only 80 mAh g^{-1} at C/10 shown in Figure 6a. When high surface area carbon such as acetylene black is milled with nano-$LiMnPO_4$, the carbon acts as a buffer to avoid too much agglomeration. It was also reported that acetylene black minimizes the damage of the carbon coating during the ball milling [39].

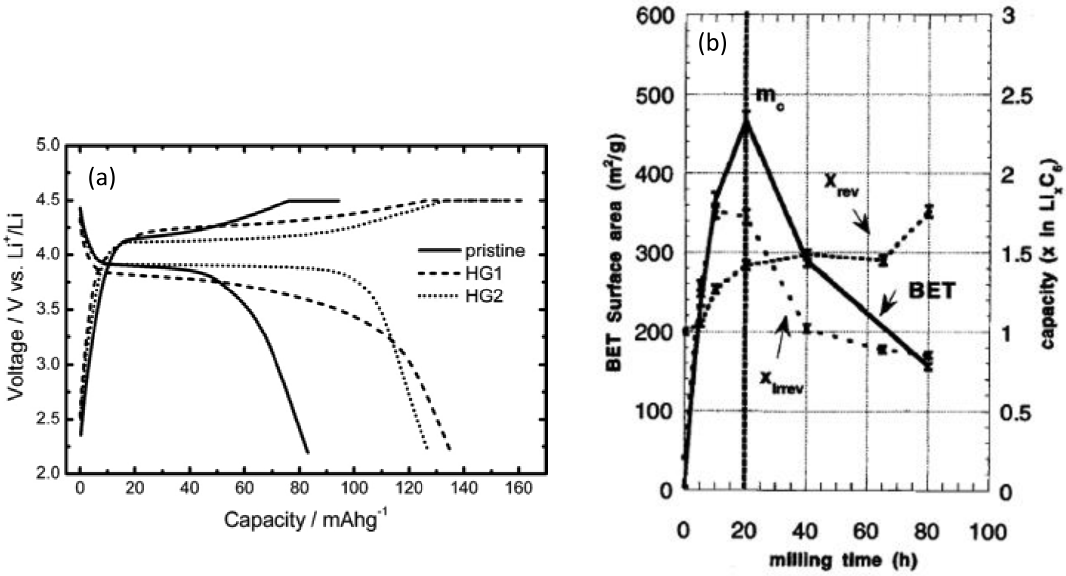

Figure 6. (**a**) The charge and discharge curves of the non-ball-milled and ball-milled $LiMnPO_4$ without (HG1) and with acetylene black (HG2) electrode [39]. (**b**) The reversible and irreversible capacities with the surface area of graphite as a function of milling time [35].

Kwon et al. prepared composites consisting of various shaped nano-$LiMnPO_4$ in particle sizes between 30–100 nm (SSA = 18–100 m^2 g^{-1}) with high surface area of Ketjen black carbon (SSA = 1400 m^2 g^{-1}) via ball milling [59]. Ketjen black carbon is rather more suitable than large particles (>1 µm) of graphite to cover the high surface area nano-$LiMnPO_4$ particles [118]. An optimization of the ball milling time was carried out with 20 wt% of Ketjen black carbon in 10 mL of stainless steel with 3 mm in diameter of 30 stainless steel balls. It showed that 1 h of milling with a frequency of 30/s provided a better homogeneity than the same duration but with a low frequency of 15/s [119].

The structures and the morphologies of SWCNT and graphitic carbon have been extensively studied as anode materials upon milling [35,120,121]. A short ball milling of CNT for 10 min increased the insertion of lithium ions into CNT, thus increasing the reversible capacity [121]. On the other hand, further milling increased the amount of disordered/amorphous carbon [35,121]. Disma et al. reported that the specific capacity of a mesocarbon microbead (MCMB) graphite anode was improved by up to 150% by ball milling with the increase of the surface area. A further milling of graphite lead to a decrease of the specific surface area and the capacity became saturated, as shown in Figure 6b [35].

Hence, the duration, force, type and amount of material/balls should be considered in ball milling in order to obtain a desired composite structure and morphology. The key advantages of ball-milled nanocomposites are their specific surface area, pore size and volume, appropriate agglomerated size, appropriate defects and surface modification in order to facilitate Li^+ and electron transport [122–126].

6. Summary of $LiMnPO_4$ Electrodes

Table 1 shows the summary of $LiMnPO_4$ electrodes prepared by different types of carbon, the total amount of carbon including the mass % of carbon within the composite, and different preparation methods to generate the carbon coating with their respective capacities. Figure 7 resumes the rate capabilities of $LiMnPO_4$ and $LiMn_{1-x}Fe_xPO_4$ electrodes. At the same C-rates for both charge and discharge, one of the highest discharge capacities of $LiMnPO_4$ reported up to date is 140, 113 and 70 mAh g^{-1} at C/10, 1C and 5C, respectively [37]. Zong et al. reported 139 and 119 mAh g^{-1} at C/20 and 1C with graphene nanoplates, but they did not show the values at higher C-rates [40]. The discharge rate capability can be increased by using a constant slow charging rate. Yoshida et al. obtained $LiMnPO_4$ discharge capacities of 150, 140 and 136 mAh g^{-1} at C/10, 1C and 5C, respectively when the charging rate was fixed to C/20 up to 4.8 V in constant current-constant voltage (CC-CV) for 35 h [73]. Other groups also obtained higher discharge capacities with constant slow charging rates (C/25 or C/10) than those obtained at the same charge and discharge rate [15,36,64,71]. The capacities and rate capability have been further increased by adding Fe in the structure of $LiMn_{1-x}Fe_xPO_4$ [91,127]. Wang et al. reported nanorods of $LiMn_{0.75}Fe_{0.25}PO_4$ grown on reduced graphene oxide that provided the discharge capacities of 153, 132, 65 mAh g^{-1} at 2C, 20C, 100C (charging for 36 s), respectively. These Fe doped $LiMn_xPO_4$ cathodes showed rate properties comparable to the other best performing cathode materials such as $LiCoO_2$, $LiFePO_4$ and $LiMn_2O_4$ [91].

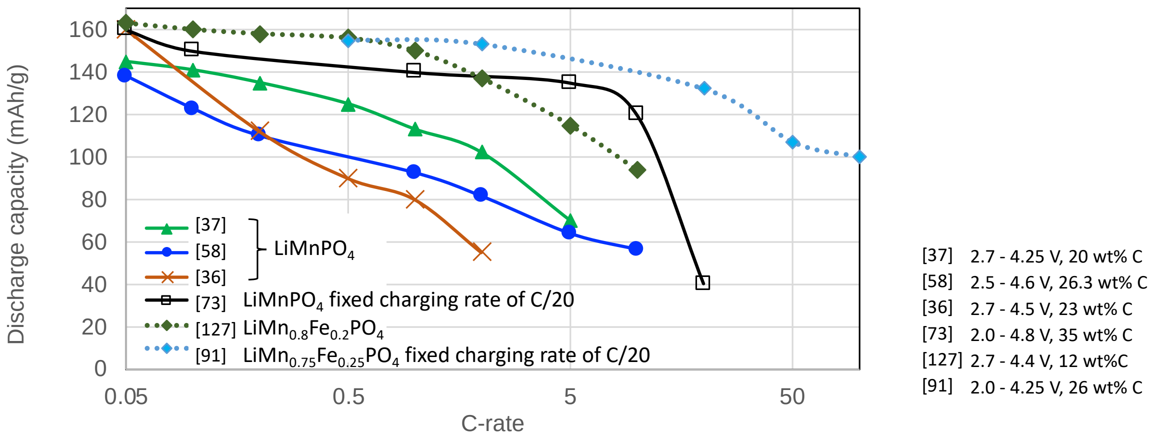

Figure 7. The summary of discharge capacities versus various C-rates of the literatures measured at the same charge C-rates as the discharge C-rates.

Table 1. The summary of $LiMnPO_4$ cathode properties with carbon type, amount of carbon and composite preparation methods.

Morphology of $LiMnPO_4$	Discharge Capacity (mAh g^{-1})	Voltage Window (V)	Carbon Type	Composite Preparation	Carbon Amount (wt%)	Reference
Round, monosize 40 nm	140, 1C, 135, 5C, 120, 10C, 40, 20C (charged at C/20)	2.0–4.8	KB + AB	BM + thermal treatment	15 + 20 (AB) = 35	[73]
Round, 10–50 nm	155, C/10, 126, 1C, 85, 5C (charged at C/20)	2.7–4.5	Sucrose + AB	BM + thermal treatment	25.5 + 7.5 = 33	[15]
Round, 15 nm crystals	142, C/10, 110, 1C, 75, 5C (charged at C/10)	2.5–4.5	Sucrose + Super P	BM + pyrolysis	0.376 (Sucrose C) + 20 = 20.4	[64]
70–100 nm (sequential precipitation)	153, C/20, 62, 5C (charged at C/25)	2.5–4.5	Sucrose + Super P	Thermal decomposition	5.95 (Sucrose C) + 20 = 25.95	[63]
180–330 nm (co-precipitation)	13, C/20 (charged at C/25)		CTAB		No carbon coating from CTAB	
Round, 50–100 nm	Graphene nanoplates: 139, C/20, 119, 1C	2.2–4.5	Graphene, AB	Slurry + planetary milling + annealing	21.25 (Graphene) + 5 = 26.25	[40]
	AB: 130, C/20, 60, 1C				25	
Platelet, 30 nm thickness	141, C/10, 113, 1C, 75, 5C	2.7–4.4	CB + graphite	Dry ball milling	18.1 (CB) + 7.5 (graphite) = 25.6	[37]
Round, 140 nm	134, C/10, 81, 1C 160, C/10, 140, 1C, 80, 5C (charged at C/20)	2.7–4.5	CB	Dry ball milling	23	[36,51]
Rod, 150–200 × 30–35 nm (27 m^2 g^{-1})	Rod: 140, C/20, 98, 1C, 65, 5C, 59, 10C	2.5–4.6	CB	Dry ball milling	26.3	[58]
Round, 30–35 nm (35 m^2 g^{-1})	Round: 80, C/20, 35 1C					
Cubic, 200–250 × 50 nm (14 m^2 g^{-1})	Cubic: 45, C/20, 17, 1C					
Plate, 50 nm	130, C/10, 54, 1C	2.0–4.5	KB + Super P	Planetary ball milling	17.5 (KB) + 2.5 = 20	[71]
	154, C/10, 117, 1C (charged at C/25)					
Polyhedral, 200–500 nm	53, C/100 @30 °C	3.0–4.5	Ascorbic acid + KB	Hydrothermal + thermal decomposition	1.875 + 15 = 16.875	[65]
	72, C/100 @30 °C		Sucrose + KB		4.125 + 15 = 19.125	
	94, C/100 @30 °C		CMC + KB		2.1 + 15 = 17.1	
	8, C/100 @30 °C		PEO + KB		0 + 15 = 15	
Plate, <100 nm × 20–30 nm (20 m^2 g^{-1})	Plate/graphene: 149, C/10, 90, 1C	2.0–4.5	Graphene, glucose, SP carbon	Spray drying, thermal decomposition	6 (glucose C) + 15 (SP) = 21	[92]
6 μm (crystals: 27–48 nm)	Non-ball-milled: 83, C/20	2.2–4.5	AB	Non-milling	10	[39]
	BM w/o C: 135, C/20, 97, 1C			High-energy ball milling		
	BM with C: 127, C/20, 100, 1C					
Plate: 35 × 400 nm (23.5 m^2 g^{-1})	Plate-CVD: 147, C/20, 110, 1C	2.9–4.9	Methylbenzene + AB	CVD	Plate: 8 + 15 (AB) = 23	[30]
Rod: 90–130 nm × 600 nm (8.8 m^2 g^{-1})	Rod-CVD: 126, C/20, 60, 1C				Rod: 11 + 15 (AB) = 26	
	Plate-BM: 126, C/20			Planetary ball milling	20 + 15 (AB) = 35	
	Rod-BM: 92, C/20					
$LiMn_{0.75}Fe_{0.25}PO_4$ Rod, 50–100 × 20–30 nm	155, C/2, 153, 2C 100, 100C (charged at C/20)	2.0–4.25	Graphene, Super P	Solution + annealing	16 (Graphene) + 10 = 26	[91]
$LiMn_{0.85}Fe_{0.15}PO_4$ 100–200 nm	Micron-composite: 140, C/10, 123, 1C, 100, 3C (charged at C/20)	2.7–4.5	Sucrose + pitch + Carbon black	Solution + annealing	3 (solution) + 2 + 7.5	[61]
	Nano: 163, C/10, 140 1C, 110, 3C (charged at C/20)		Sucrose + AB+CB	ultrasonic spray pyrolysis+ BM with carbon+annealing	30 (AB) + 7.5 (CB)	

AB: Acetylene black, CB: Carbon black, CMC: carboxymethyl cellulose, CNT: Carbon nanotube, CTAB: cetyltrimethyl ammonium bromide, KB: Ketjen black, PEO: Polyethylene oxide.

7. Carbonaceous Materials in the Composite of $LiCoO_2$/C

$LiCoO_2$ is the first successful cathode material of Li-ion batteries because of its high electronic and ionic conductivities, and one of the best preforming cathodes although the practical capacity of 140 mAh g^{-1} corresponds to only ca. 50% of the theoretical value (274 mAh g^{-1}) due to the structural changes upon further de-lithiation [2]. Different types of carbon have been studied in composites with micron-sized $LiCoO_2$ particles: graphite ('SFG' [128], 'SLC' [128], and 'KS6' [10,129]), carbon black (Ketjen black [128], 'C65' or Super P [10,20,23,42,128–130], acetylene black [10,20,22,41,131]), vapor deposit carbon fibers (VCF) [41], and CNT [41,42,86,129].

The properties of $LiCoO_2$ cathodes with different types and amounts of carbon are summarized with their capacities in Table 2.

Figure 8a–d show TEM images of various types of carbonaceous materials. While SFG presents itself as thin plates of graphite, SLC is made of large compact spherical graphite particles. Ketjen black forms highly porous nanoparticles of the order of ca. 20–30 nm, while C65 has non-porous particles with a diameter of ca. 100 nm. Kwon et al. prepared composites of each carbon and micron-sized $LiCoO_2$ via ball milling, and Figure 8e,f show the largest difference of the composite structures consisting of Ketjen black and SFG, respectively. For comparison, the composites were always ball-milled (30 s^{-1}) with 20 wt% carbon based on round-shaped and micron sized $LiCoO_2$ for 1 h. During the ball milling process, the highly porous and nano-sized Ketjen black was strongly aggregated, reduced its specific surface area and segregated from $LiCoO_2$. In the end, the carbon formed a thick and dense layer on the surface of $LiCoO_2$ (indicated with arrows in Figure 8e). This thick and dense carbon layer has a low lithium ion permeability, resulting in a lower specific capacity [128]. On the other hand, the platelet-shaped SFG graphite agglomerated less and formed a thin layer of carbon on the active material particles, resulting in easier penetration of lithium ions. Thus, large sized graphitic SFG and SLC were better mixed with micron-sized $LiCoO_2$ while nano-sized spherical-shaped Ketjen black and C65 were segregated and the carbon coating layer was thicker. The initially micron-sized $LiCoO_2$ particles were in all cases reduced in size during ball milling (bright color in SEM). Finally, the agglomerated dense composite were formed, consisting of submicron sized $LiCoO_2$ and carbon as shown in Figure 8e,f.

Table 2. The comparison of composite $LiCoO_2$/C cathode with different types and amounts of carbon and their capacities.

$LiCoO_2$	Capacity (mAh g^{-1})	Voltage Window (V)	Carbon Type	Composite Preparation	Carbon Amount (wt%)	Reference
40 µm, platelet	169, C/5, 164, 3C	3–4.5	Super P	Slurry mixing	4	[130]
10 µm	145, C/5	2.75–4.2	Super P	Wet BM with orotan™	2	[23]
10 µm	155, C/10, 127, 2C	3–4.3	Super P	Slurry mixing	10	[129]
	155, C/10, 137, 2C		Super-aligned CNT	Ultrasonication in solvent	5	
Micron	136, C/2	3–4.125	Super P/Lonza	Pestle	10	[10]
	130, C/2		Lonza			
	125, C/2		Super P			
Submicron	125, C/2	2.5–4.35	Super P/AB	Mixing with binder	6, 6	[132]
10–20 µm	157, C/10, 148, 1C	3–4.3	Super P	Slurry mixing	8	[42]
	157, C/10, 148, 1C		MWCNT			
Micron	130, C/10, 120, 1C	3–4.3	Sucrose and AB	Planet milling + thermal decomposition	5	[22]
LT-LCO	105, C/5, 93, 1C	2.7–4.2	AB and natural graphite	Pellet	7 + 7	[133]
HT-LCO	121. C/5, 75, 1C					
Micron, round	140, C/10, 120, 1C	3–4.3	CNT	Agate mortar (slurry mixing)	3	[41]
	125, C/10, 100, 1C		AB		3	
	135, C/10, 103, 1C		Chemical VCF		3	
Submicron	220, C/10, 106, 1C	2.7–4.4	SFG	BM	10	[134]
	156, C/10, 109, 1C		KB		10	

AB: acetylene black, BM: ball milling, CB: carbon black, CNT: carbon nanotube, LT-LCO: low-temperature $LiCoO_2$, HT-LCO: high-temperature $LiCoO_2$, MWCNT: multi-walled CNT, KB: Ketjen black, VCF: vapor deposited carbon fibers.

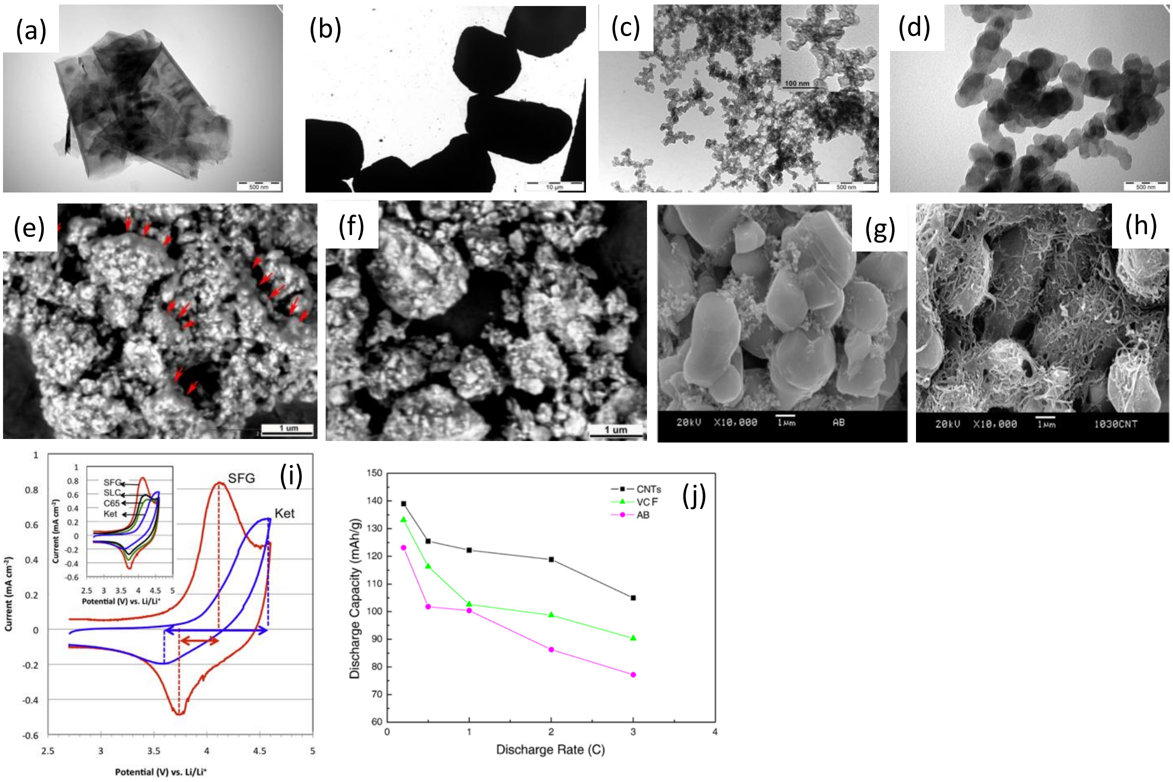

Figure 8. (**a**–**d**) TEM images of various carbon morphologies: (**a**) SFG platelet-shaped graphite, (**b**) SLC spherical graphite, (**c**) Ketjen black, highly porous and nanosized spherical carbon black and (**d**) C65, spherical carbon black [128]. (**e**–**h**) SEM images of composites: backscattered images of the ball-milled composites (**e**) Ketjen black carbon black-$LiCoO_2$, (**f**) SFG graphite-$LiCoO_2$ [128], (**g**) acetylene black-$LiCoO_2$, (**h**) CNT-$LiCoO_2$ [41]. (**i**) Cyclic voltammograms (CVs) of $LiCoO_2$ composite electrodes consisting of Ketjen black or SFG carbon. Inset is CVs of $LiCoO_2$ electrodes with SFG, SLC, C65 and Ketjen black carbon [128]. (**j**) The discharge capacities of the composite $LiCoO_2$ with CNT, VCF or acetylene black carbon at various discharge rates [41].

Complementary to this study, Hong et al. [10] reported that the density and particle size of carbon affected the mixing efficiency with $LiCoO_2$. Lonza KS6 was better mixed with $LiCoO_2$ than carbon black because the density of the former (2.2 g cm^{-3}) is heavier than that of the latter (1.8 g cm^{-3}) so the lighter carbon black tends to segregate while the heavier $LiCoO_2$ particles (4.9 g cm^{-3}) settled down in the mixing step [10]. They also reported that the similar particle sizes between carbon and $LiCoO_2$ are an important parameter to disperse the electrode components.

Three, yet different types of conductive nano-carbon additives have been reported in a complementary study by Guoping et al., also in combination with micron-sized $LiCoO_2$. Wire-shaped CNT, chemical vapor deposited carbon fibers (VCF) and spherical-shaped acetylene black carbon were mixed with $LiCoO_2$ via the slurry procedure. Spherical nano-sized acetylene black carbon provided a poor mixing with $LiCoO_2$ particles (Figure 8g) while the CNT additive lead to a continuous conductive network in the composite (Figure 8h) [41]. The homogeneous composite structure improved the electronic conductivity, resulting in higher charge/discharge capacity. As CNT are very flexible and electronically conductive, this material can play a role of both a binder and a current collector, which can increase mass and volume capacities compared to the cathodes with a binder and Al current collector [129]. Varzi et al. studied $LiNi_{0.33}Mn_{0.33}Co_{0.33}O_2$ (hereafter referred to as NMC) with 1 wt% of MWCNT replacing 4 wt% of carbon black in the electrode. The capacity of NMC was increased to 87 mAh/g using MWCNT at 5C in comparison to 58 mAh/g for carbon black. On the other hand, they reported that CNT showed a large capacity fading at the low voltage range such as <1.0 V vs. Li^+/Li [86].

Apart from the particle sizes of carbon and $LiCoO_2$ before and after ball milling, another important parameter characterizing the composite and hence the battery performance is related to the specific surface area of the composite. For example, using Ketjen black leads to an overall reduced specific surface area of the composite (SSA = 22.27 $m^2 g^{-1}$), while using SFG in the composite, in spite of its larger carbon particles (SSA = 16 $m^2 g^{-1}$) to start with, leads to a larger surface area of 35.82 $m^2 g^{-1}$ in the end [128]. A lower surface area of the composite means a reduced number of particles and smaller pores between them. Hence the contact between the composite and the liquid electrolyte is reduced, hindering the penetration of liquid electrolyte into the electrode. Therefore, we found that the electrochemical properties of these four different composites are very different as shown in Figure 8i. The best property for the $LiCoO_2$ electrodes was obtained using platelet-shaped SFG graphite via dry ball milling. This study revealed that the change in composite structure depending on the carbon materials was directly related to the battery properties.

In summary, the segregation and pore closing occurred with lighter and high surface area of Ketjen black carbon and C65 carbon during ball milling while heavier and large surface area of SFG and SLC graphitic carbon was better mixed with micron sized $LiCoO_2$. The relation between a high surface area of Ketjen black carbon (SSA = 1400 $m^2 g^{-1}$) and larger sized $LiCoO_2$ (SSA = 0.52 $m^2 g^{-1}$) resulted in inhomogeneous mixing due to the large difference of sizes and powder densities between two materials. The homogeneity and the composite structure can be influenced by the duration of ball milling. The carbon characteristics before and after ball milling are described in the next section.

8. Characteristics of Carbon in Ball-Milled Composite of $LiCoO_2$/C

The mixing efficiency between the electrode ingredients can be varied by ball milling types such as planetary, attrition, spex, rotational milling etc. Among those milling methods, one can again differentiate between wet or dry state milling, depending on the addition of solvent or not. In general, a wet milling with a solvent provides less segregation/agglomeration than a dry one but it may require a surface modification of one component to adhere to the other component. In general though, the mixing efficiency is poorer for wet than for a dry milling [135]. On the other hand, a dry milling does not contain a solvent and more physical and direct contacts of particle-ball, particle-particle or particle-wall of the container occur than in a wet milling. For dry milling, the mixing efficiency can be controlled by an input energy (speed of vibration or movement), ball size, a number of balls, milling time etc.

The variation of dry ball milling conditions has been investigated in order to maximize the properties of $LiCoO_2$ electrodes. Figure 9 shows the cyclic voltammograms of $LiCoO_2$ electrodes using the composites containing SFG, respectively Ketjen black prepared by ball milling for various milling times at 30 s^{-1}. Each electrode contains this time 10 wt% of carbon. 5 min of ball milling turned out to be the best condition to obtain the maximum redox reaction of $LiCoO_2$ electrode in both cases, leading to well-determined redox reactions and high current densities.

However, under the same ball milling condition of 5 min, SFG graphite provided significantly higher specific capacities of about 230 and 200 mAh g^{-1} at C/10 and C/5, respectively, while the specific capacity of $LiCoO_2$ with Ketjen black carbon was about 150 and 140 mAh g^{-1} at the same C-rates, respectively. The ionic diffusion analysis also showed the highest diffusion coefficient of Li^+ in the composite, which was ball-milled for 5 min. A longer milling time (>30 min) degraded the electrochemical properties in all types of composites.

Figure 10a shows the Raman spectra of SFG graphite and Ketjen black carbon using various ball milling times. The signals of amorphous carbon and graphite show a clear difference of intensities, widths and the intensity ration of I(D)/I(G) between ordered (G) and disordered (D) positions [136–139]. The initial carbon structure of SFG graphite showed much stronger intensity of the ordered C–C band at 1600 cm^{-1} than that of the disordered C–C band at 1350 cm^{-1} before ball milling. When graphite was ball-milled, the ordered structure is reduced as observed by the decreased intensity of the G band and the increased disordered position [140]. This indicates that the ordered structure gets damaged when ball milling lasts longer than 5 min. On the other hand, Ketjen black carbon has a higher intensity of the disordered band, D, than that of the ordered band in Figure 10b at the initial state. Upon milling, the ratio of D and G does not change much but the intensities of both D and G bands are lowered.

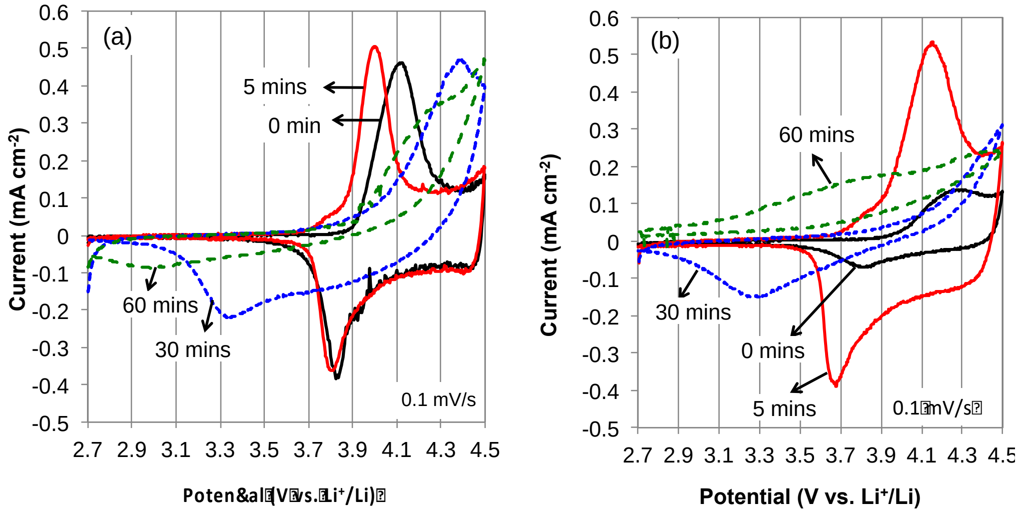

Figure 9. Cyclic voltammograms of $LiCoO_2$ electrodes using (**a**) the composite of $LiCoO_2$ and SFG graphite and (**b**) the composite of $LiCoO_2$ and Ketjen black prepared by a dry ball milling for various milling times [134].

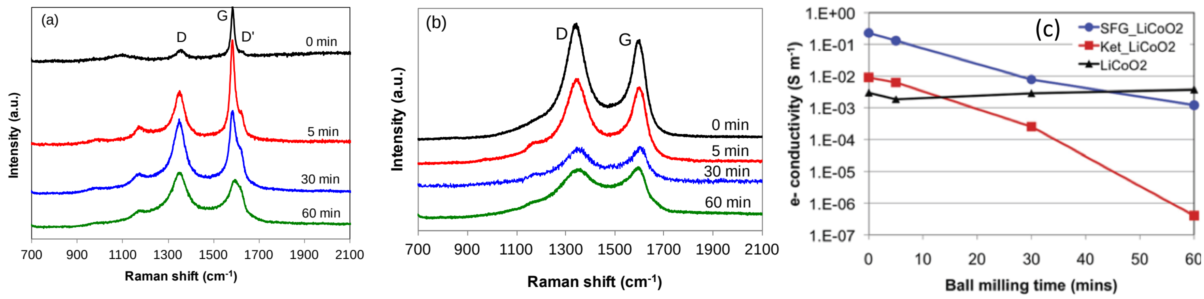

Figure 10. Raman spectra of SFG (**a**) and Ketjen black (**b**) carbon in the composites prepared in various ball milling time and (**c**) electronic conductivities of the composites and $LiCoO_2$ alone in terms of milling time [134].

The electronic conductivities of those composites decreased upon ball milling in both cases of SFG graphite and Ketjen black as shown in Figure 10c, which corresponds well to the results of Raman spectroscopy upon milling. The reasons for the lowered performance of the composites prepared by a longer milling time revealed (1) the segregation and pore closing of the composite in case of Ketjen black carbon, and (2) the increase of the disordered D-band structure of sp^3-hybridized carbon atoms after a longer milling time, as found by Raman spectroscopy (Figure 10b), while (3) a 4-point probe conductivity measurement further confirmed that the electronic conductivity of the composites decreases upon milling time (Figure 10c) [134].

Therefore, in order to obtain high performance electrodes, several characteristics of the composite, in particular a homogeneous structure, good electronic conductivity and high enough surface area (porosity) have to be considered. Those combined characteristics provide the permeability and electrochemical reaction kinetics of Li^+ and e^- to store and produce electrical energy of lithium ion batteries [126].

9. Conclusions

Cathode performance and properties depend on the structure and morphology of the composite, related to both the initial and final physicochemical characteristics. In order to achieve high performance of Li-ion batteries, the major characteristics of the cathode are its high electrical and ionic conductivities to allow fast transport of a large number of electrons and lithium ions in a certain time of charge and discharge. These conductivities can be maximized by generating a continuous network between the composite materials and by obtaining a porous structure to allow access for the electrolyte into the electrode. Many battery electrode materials require improvement of their electronic conductivity. Carbon is then added as a conductive material. We reviewed that the carbon sources, the structure of carbon contained in the composite, and the methods of making the composites using those carbon composite materials all affected the final battery properties and characterizations. The properties of a composite depend on the fabrication process of the composite. Among several methods to make carbon coatings on the redox active materials, we lay special focus on ball milling. The major advantages of composites prepared by ball milling are the homogeneous mixing, composite size, appropriate pore size/volume, and appropriate defects of carbon and surface modifications formed in different atmospheres. Also, the initial characteristics of carbon such as size, shape, porosity of carbon, and structure of carbon (graphite or carbon black) are affected by the condition of ball milling. Ball milling can be used to achieve a homogenous and dense mixing via the right choice of carbon and optimization of the process. As we have shown that SFG graphite is the best for micron and submicron-$LiCoO_2$ while high surface area carbon such as Ketjen black is the best for nano-$LiMnPO_4$ in the ball milling process, there is no single type of carbon recommendable to all electrode materials. Choosing similar particle sizes of carbon and the active material can be one way to provide better homogeneous mixing and high conductivity in the composite. Also, the amount and shape of carbon in a composite govern the electronic conductivity and the volumetric capacity of the electrode. The desired composite structure should allow Li^+ and electrons to be transported into the electrolyte and the current collector, respectively.

Overall, there are many studies on active materials mixed with carbon, but rare are the systematic studies that allow direct comparisons between the results given in the literature. Yet, it could be seen that investigating the best conditions for the generation of the electrode composites can make a big difference in the final properties of the electrodes.

Author Contributions: N.H.K. created the concept and the original draft of the manuscript. D.M.-M. searched literatures. K.M.F. reviewed and commented on the manuscript.

Funding: The authors thank the Swiss National Science Foundation for funding (NRP 64 and NRP 70) and the Swiss Center for Competence in Energy Research (SCCER) Heat and Electricity Storage (contract No. 1155000153). We also thank the University of Fribourg and EKZ (Elektrizitätswerke des Kantons Zürich) for the innovation grant.

Conflicts of Interest: The authors declare there is no conflict of interest regarding the publication of the manuscript.

References

1. Schmuch, R.; Wagner, R.; Hörpel, G.; Placke, T.; Winter, M. Performance and cost of materials for lithium-based rechargeable automotive batteries. *Nat. Energy* **2018**, *3*, 267–278. [CrossRef]
2. Whittingham, M.S. Lithium batteries and cathode materials. *Chem. Rev.* **2004**, *104*, 4271–4301. [CrossRef] [PubMed]
3. Nazri, G.-A.; Pistoia, G. *Lithium Batteries: Science and Technology*; Kluwer Academic Publishers: Norwell, MA, USA, 2004.
4. Megahed, S.; Scrosati, B. Lithium-ion rechargeable batteries. *J. Power Sources* **1994**, *51*, 79–104. [CrossRef]
5. Wakihara, M. Recent developments in lithium ion batteries. *Mater. Sci. Eng. R-Rep.* **2001**, *33*, 109–134. [CrossRef]
6. Goodenough, J.; Park, K.-S. The Li-ion rechargeable battery: A perspective. *J. Am. Chem. Soc.* **2013**, *135*, 1167–1176. [CrossRef] [PubMed]

7. Tukamoto, H.; West, A.R. Electronic conductivity of $LiCoO_2$ and its enhancement by magnesium doping. *J. Electrochem. Soc.* **1997**, *144*, 3164–3168. [CrossRef]
8. Levasseur, S.; Ménétrier, M.; Delmas, C. On the Dual Effect of Mg Doping in $LiCoO_2$ and $Li_{1+\delta}CoO_2$: Structural, Electronic Properties, and ^{7}Li MAS NMR Studies. *Chem. Mater.* **2002**, *14*, 3584–3590. [CrossRef]
9. Prosini, P.P.; Zane, D.; Pasquali, M. Improved electrochemical performance of a $LiFePO_4$-based composite cathode. *Electrochim. Acta* **2001**, *46*, 3517–3523. [CrossRef]
10. Hong, J.K.; Lee, J.H.A.; Oh, S.M. Effect of carbon additive on electrochemical performance of $LiCoO_2$ composite cathodes. *J. Power Sources* **2002**, *111*, 90–96. [CrossRef]
11. Dominko, R.; Gaberscek, M.; Drofenik, J.; Bele, M.; Jamnik, J. Influence of carbon black distribution on performance of oxide cathodes for Li ion batteries. *Electrochim. Acta* **2003**, *48*, 3709–3716. [CrossRef]
12. Im, D.; Manthiram, A. Lithium manganese oxide-conductive carbon nanocomposite cathodes for rechargeable lithium batteries. *Solid State Ion.* **2003**, *159*, 249–255. [CrossRef]
13. Myung, S.T.; Komaba, S.; Takagai, R.; Kumagai, N.; Lee, Y.S. Emulsion drying preparation of $LiFePO_4/C$ composite and its enhanced high-rate performance at 50 °C. *Chem. Lett.* **2003**, *32*, 566–567. [CrossRef]
14. Bakenov, Z.; Taniguchi, I. Physical and electrochemical properties of $LiMnPO_4/C$ composite cathode prepared with different conductive carbons. *J. Power Sources* **2010**, *195*, 7445–7451. [CrossRef]
15. Oh, S.-M.; Oh, S.-W.; Yoon, C.-S.; Scrosati, B.; Amine, K.; Sun, Y.-K. High-Performance Carbon-$LiMnPO_4$ Nanocomposite Cathode for Lithium Batteries. *Adv. Funct. Mater.* **2010**, *20*, 3260–3265. [CrossRef]
16. Ni, H.; Liu, J.; Fan, L.-Z. Carbon-coated $LiFePO_4$-porous carbon composites as cathode materials for lithium ion batteries. *Nanoscale* **2013**, *5*, 2164–2168. [CrossRef] [PubMed]
17. Norberg, N.S.; Kostecki, R. Interfacial phenomena at a composite $LiMnPO_4$ cathode. *J. Electrochem. Soc.* **2012**, *159*, A1091–A1094. [CrossRef]
18. Babinec, S.; Tang, H.; Talik, A.; Hughes, S.; Meyers, G. Composite cathode structure/property relationships. *J. Power Sources* **2007**, *174*, 508–514. [CrossRef]
19. Manickam, M.; Takata, M. Effect of cathode binder on capacity retention and cycle life in transition metal phosphate of a rechargeable lithium battery. *Electrochim. Acta* **2003**, *48*, 957–963. [CrossRef]
20. Spahr, M.E.; Goers, D.; Leone, A.; Stallone, S.; Grivei, E. Development of carbon conductive additives for advanced lithium ion batteries. *J. Power Sources* **2011**, *196*, 3404–3413. [CrossRef]
21. Kim, H.-S.; Kong, M.; Kim, K.; Kim, I.-J.; Gu, H.-B. Effect of carbon coating on $LiNi_{1/3}Mn_{1/3}Co_{1/3}O_2$ cathode material for lithium secondary batteries. *J. Power Sources* **2007**, *171*, 917–921. [CrossRef]
22. Cao, Q.; Zhang, H.P.; Wang, G.J.; Xia, Q.; Wu, Y.P.; Wu, H.Q. A novel carbon-coated $LiCoO_2$ as cathode material for lithium ion battery. *Electrochem. Commun.* **2007**, *9*, 1228–1232. [CrossRef]
23. Kim, J.; Kim, B.; Lee, J.-G.; Cho, J.; Park, B. Direct carbon-black coating on $LiCoO_2$ cathode using surfactant for high-density Li-ion cell. *J. Power Sources* **2005**, *139*, 289–294. [CrossRef]
24. Chen, Z.H.; Dahn, J.R. Reducing carbon in $LiFePO_4/C$ composite electrodes to maximize specific energy, volumetric energy, and tap density. *J. Electrochem. Soc.* **2002**, *149*, A1184–A1189. [CrossRef]
25. Cushing, B.L.; Goodenough, J.B. Influence of carbon coating on the performance of a $LiMn_{0.5}Ni_{0.5}O_2$ cathode. *Solid State Sci.* **2002**, *4*, 1487–1493. [CrossRef]
26. Zhang, H.-L.; Liu, S.-H.; Li, F.; Bai, S.; Liu, C.; Tan, J.; Cheng, H.-M. Electrochemical performance of pyrolytic carbon-coated natural graphite spheres. *Carbon* **2006**, *44*, 2212–2218. [CrossRef]
27. Marinho, B.; Ghislandi, M.; Tkalya, E.; Koning, C.E.; de With, G. Electrical conductivity of compacts of graphene, multi-wall carbon nanotubes, carbon black, and graphite powder. *Powder Technol.* **2012**, *221*, 351–358. [CrossRef]
28. Wang, Y.; Liu, H.T.; Cheng, H.F. Characterisation of CVD carbon coatings on Nextel^{TM} 440 fibres. *Surf. Eng.* **2016**, *32*, 218–222. [CrossRef]
29. Takahara, H.; Takeuchi, T.; Tabuchi, M.; Kageyama, H.; Kobayashi, Y.; Kurisu, Y.; Kondo, S.; Kanno, R. All-solid-state lithium secondary battery using oxysulfide glass. *J. Electrochem. Soc.* **2004**, *151*, A1539–A1544. [CrossRef]
30. Wang, F.; Yang, J.; Gao, P.; NuLi, Y.; Wang, J. Morphology regulation and carbon coating of $LiMnPO_4$ cathode material for enhanced electrochemical performance. *J. Power Sources* **2011**, *196*, 10258–10262. [CrossRef]
31. Han, Y.-S.; Lee, J.-Y. Improvement on the electrochemical characteristics of graphite anodes by coating of the pyrolytic carbon using tumbling chemical vapor deposition. *Electrochim. Acta* **2003**, *48*, 1073–1079. [CrossRef]

32. Ding, Y.-S.; Li, W.-N.; Iaconetti, S.; Shen, X.-F.; DiCarlo, J.; Galasso, F.S.; Suib, S.L. Characteristics of graphite anode modified by CVD carbon coating. *Surf. Coat. Technol.* **2006**, *200*, 3041–3048. [CrossRef]
33. Fu, K.; Xue, L.; Yildiz, O.; Li, S.; Lee, H.; Li, Y.; Xu, G.; Zhou, L.; Bradford, P.D.; Zhang, X. Effect of CVD carbon coatings on Si@CNF composite as anode for lithium-ion batteries. *Nano Energy* **2013**, *2*, 976–986. [CrossRef]
34. Yu, J.; Yang, J.; Feng, X.; Jia, H.; Wang, J.; Lu, W. Uniform Carbon Coating on Silicon Nanoparticles by Dynamic CVD Process for Electrochemical Lithium Storage. *Ind. Eng. Chem. Res.* **2014**, *53*, 12697–12704. [CrossRef]
35. Disma, F.; Aymard, L.; Dupont, L.; Tarascon, J.-M. Effect of Mechanical Grinding on the Lithium Intercalation Process in Graphites and Soft Carbons. *J. Electrochem. Soc.* **1996**, *143*, 3959–3972. [CrossRef]
36. Kwon, N.-H.; Drezen, T.; Exnar, I.; Teerlinck, I.; Isono, M.; Graetzel, M. Enhanced electrochemical performance of mesoparticulate $LiMnPO_4$ for lithium ion batteries. *Elecrochem. Solid State Lett.* **2006**, *9*, A277–A280. [CrossRef]
37. Wang, D.; Buqa, H.; Crouzet, M.; Deghenghi, G.; Drezen, T.; Exnar, I.; Kwon, N.-H.; Miners, J.H.; Poletto, L.; Grätzel, M. High-performance, nano-structured $LiMnPO_4$ synthesized via a polyol method. *J. Power Sources* **2009**, *189*, 624–628. [CrossRef]
38. Dettlaff-Weglikowska, U.; Sato, N.; Yoshida, J.; Roth, S. Preparation and electrochemical characterization of $LiMnPO_4$/single-walled carbon nanotube composites as cathode material for Li-ion battery. *Phys. Status Solidi B* **2009**, *246*, 2482–2485. [CrossRef]
39. Ni, J.; Kawabe, Y.; Morishita, M.; Watada, M.; Sakai, T. Improved electrochemical activity of $LiMnPO_4$ by high-energy ball-milling. *J. Power Sources* **2011**, *196*, 8104–8109. [CrossRef]
40. Zong, J.; Liu, X. Graphene nanoplates structured $LiMnPO_4$/C composite for lithium-ion battery. *Electrochim. Acta* **2014**, *116*, 9–18. [CrossRef]
41. Guoping, W.; Qingtang, Z.; Zuolong, Y.; Meizheng, Q. The effect of different kinds of nano-carbon conductive additives in lithium ion batteries on the resistance and electrochemical behavior of the $LiCoO_2$ composite cathodes. *Solid State Ion.* **2008**, *179*, 263–268. [CrossRef]
42. Park, J.H.; Lee, S.-Y.; Kim, J.H.; Ahn, S.; Park, J.-S.; Jeong, Y.U. Effect of conducting additives on the properties of composite cathodes for lithium-ion batteries. *J. Solid State Electrochem.* **2009**, *14*, 593–597. [CrossRef]
43. Jiao, F.; Bao, J.; Hill, A.H.; Bruce, P.G. Synthesis of ordered mesoporous Li-Mn-O spinel as a positive electrode for rechargeable lithium batteries. *Angew. Chem.* **2008**, *47*, 9711–9716. [CrossRef] [PubMed]
44. Zhu, S.; Li, J.; Ma, L.; Guo, L.; Li, Q.; He, C.; Liu, E.; He, F.; Shi, C.; Zhao, N. Three-Dimensional Network of N-Doped Carbon Ultrathin Nanosheets with Closely Packed Mesopores: Controllable Synthesis and Application in Electrochemical Energy Storage. *ACS Appl. Mater. Interfaces* **2016**, *8*, 11720–11728. [CrossRef] [PubMed]
45. Zhou, F.; Kang, K.S.; Maxisch, T.; Ceder, G.; Morgan, D. The electronic structure and band gap of $LiFePO_4$ and $LiMnPO_4$. *Solid State Commun.* **2004**, *132*, 181–186. [CrossRef]
46. Yonemura, M.; Yamada, A.; Takei, Y.; Sonoyama, N.; Kanno, R. Comparative kinetic study of olivine $LixMPO_4$ (M = Fe, Mn). *J. Electrochem. Soc.* **2004**, *151*, A1352–A1356. [CrossRef]
47. Delacourt, C.; Laffont, L.; Bouchet, R.; Wurm, C.; Leriche, J.B.; Morcrette, M.; Tarascon, J.M.; Masquelier, C. Toward understanding of electrical limitations (electronic, ionic) in $LiMPO_4$ (M = Fe, Mn) electrode materials. *J. Electrochem. Soc.* **2005**, *152*, A913–A921. [CrossRef]
48. Kumar, P.R.; Venkateswarlu, M.; Manjusri, M.; Amar, K.M.; Satyanarayana, N. Enhanced conductivity and electrical relaxation studies of carbon-coated $LiMnPO_4$ nanorods. *Ionics* **2012**, *19*, 461–469. [CrossRef]
49. Kumar, P.R.; Venkateswarlu, M.; Misra, M.; Mohanty, A.K.; Satyanarayana, N. Carbon coated $LiMnPO_4$ nanorods for lithium batteries. *J. Electrochem. Soc.* **2011**, *158*, A227–A230. [CrossRef]
50. Barpanda, P.; Djellab, K.; Recham, N.; Armand, M.; Tarascon, J.-M. Direct and modified ionothermal synthesis of $LiMnPO_4$ with tunable morphology for rechargeable Li-ion batteries. *J. Mater. Chem.* **2011**, *21*, 10143–10152. [CrossRef]
51. Drezen, T.; Kwon, N.-H.; Bowen, P.; Teerlinck, I.; Isono, M.; Exnar, I. Effect of particle size on $LiMnPO_4$ cathodes. *J. Power Sources* **2007**, *174*, 949–953. [CrossRef]
52. Islam, M.S.; Driscoll, D.J.; Fisher, C.A.J.; Slater, P.R. Atomic-Scale Investigation of Defects, Dopants, and Lithium Transport in the $LiFePO_4$ Olivine-Type Battery Material. *Chem. Mater.* **2005**, *17*, 5085–5092. [CrossRef]

53. Fisher, C.A.J.; Islam, M.S. Surface structures and crystal morphologies of $LiFePO_4$: Relevance to electrochemical behaviour. *J. Mater. Chem.* **2008**, *18*, 1209–1215. [CrossRef]
54. Fisher, C.A.J.; Hart Prieto, V.M.; Islam, M.S. Lithium Battery Materials $LiMPO_4$ (M = Mn, Fe, Co, and Ni): Insights into Defect Association, Transport Mechanisms, and Doping Behavior. *Chem. Mater.* **2008**, *20*, 5907–5915. [CrossRef]
55. Guo, B.; Ruan, H.; Zheng, C.; Fei, H.; Wei, M. Hierarchical $LiFePO_4$ with a controllable growth of the (010) facet for lithium-ion batteries. *Sci. Rep.* **2013**, *3*, 2788–2793. [CrossRef] [PubMed]
56. Martha, S.K.; Markovsky, B.; Grinblat, J.; Gofer, Y.; Haik, O.; Zinigrad, E.; Aurbach, D.; Drezen, T.; Wang, D.; Deghenghi, G.; et al. $LiMnPO_4$ as an Advanced Cathode Material for Rechargeable Lithium Batteries. *J. Electrochem. Soc.* **2009**, *156*, A541–A552. [CrossRef]
57. Zane, D.; Carewska, M.; Scaccia, S.; Cardellini, F.; Prosini, P.P. Factor affecting rate performance of undoped $LiFePO_4$. *Electrochim. Acta* **2004**, *49*, 4259–4271. [CrossRef]
58. Kwon, N.H.; Yin, H.; Vavrova, T.; Lim, J.H.W.; Steiner, U.; Grobéty, B.; Fromm, K.M. Nanoparticle shapes of $LiMnPO_4$, Li^+ diffusion orientation and diffusion coefficients for high volumetric energy Li^+ ion cathodes. *J. Power Sources* **2017**, *342*, 231–240. [CrossRef]
59. Kwon, N.-H.; Fromm, K.M. Enhanced electrochemical performance of <30 nm sized $LiMnPO_4$ nanoparticles with a reduced amount of carbon as a cathode for lithium ion batteries. *Electrochim. Acta* **2012**, *69*, 38–44. [CrossRef]
60. Oh, S.W.; Myung, S.-T.; Bang, H.J.; Yoon, C.S.; Amine, K.; Sun, Y.-K. Nanoporous Structured $LiFePO_4$ with Spherical Microscale Particles Having High Volumetric Capacity for Lithium Batteries. *Electrochem. Solid-State Lett.* **2009**, *12*, A181–A185. [CrossRef]
61. Sun, Y.K.; Oh, S.M.; Park, H.K.; Scrosati, B. Micrometer-sized, nanoporous, high-volumetric-capacity $LiMn_{0.85}Fe_{0.15}PO_4$ cathode material for rechargeable lithium-ion batteries. *Adv. Mater.* **2011**, *23*, 5050–5054. [CrossRef] [PubMed]
62. Yang, J.S.; Xu, J.J. Synthesis and characterization of carbon-coated lithium transition metal phosphates $LiMPO_4$ (M = Fe, Mn, Co, Ni) prepared via a nonaqueous sol-gel route. *J. Electrochem. Soc.* **2006**, *153*, A716–A723. [CrossRef]
63. Kim, T.-H.; Park, H.-S.; Lee, M.-H.; Lee, S.-Y.; Song, H.-K. Restricted growth of $LiMnPO_4$ nanoparticles evolved from a precursor seed. *J. Power Sources* **2012**, *210*, 1–6. [CrossRef]
64. Zhao, M.; Fu, Y.; Xu, N.; Li, G.; Wu, M.; Gao, X. High performance $LiMnPO_4$/C prepared by a crystallite size control method. *J. Mater. Chem. A* **2014**, *2*, 15070–15077. [CrossRef]
65. Mizuno, Y.; Kotobuki, M.; Munakata, H.; Kanamura, K. Effect of carbon source on electrochemical performance of carbon coated $LiMnPO_4$ cathode. *J. Ceram. Soc. Jpn.* **2009**, *117*, 1225–1228. [CrossRef]
66. Yang, S.-L.; Ma, R.-G.; Hu, M.-J.; Xi, L.-J.; Lu, Z.-G.; Chung, C.Y. Solvothermal synthesis of nano-$LiMnPO_4$ from Li_3PO_4 rod-like precursor: Reaction mechanism and electrochemical properties. *J. Mater. Chem.* **2012**, *22*, 25402–25408. [CrossRef]
67. Wang, Y.; Yang, Y.; Yang, Y.; Shao, H. Enhanced electrochemical performance of unique morphological $LiMnPO_4$/C cathode material prepared by solvothermal method. *Solid State Commun.* **2010**, *150*, 81–85. [CrossRef]
68. Rangappa, D.; Sone, K.; Zhou, Y.; Kudo, T.; Honma, I. Size and shape controlled $LiMnPO_4$ nanocrystals by a supercritical ethanol process and their electrochemical peroperties. *J. Mater. Chem.* **2011**, *21*, 15813–15818. [CrossRef]
69. Maldonado-Hodar, F.J.; Moreno-Castilla, C.; Rivera-Utrilla, J.; Hanzawa, Y.; Yamada, A. Catalytic Graphitization of Carbon Aerogels by Transition Metals. *Langmuir* **2000**, *16*, 4367–4373. [CrossRef]
70. Lee, C.J.; Park, J.; Yu, J.A. Catalyst effect on carbon nanotubes synthesized by thermal chemical vapor deposition. *Chem. Phys. Lett.* **2002**, *360*, 250–255. [CrossRef]
71. Choi, D.; Wang, D.; Bae, I.T.; Xiao, J.; Nie, Z.; Wang, W.; Viswanathan, V.V.; Lee, Y.J.; Zhang, J.G.; Graff, G.L.; et al. $LiMnPO_4$ nanoplate grown via solid-state reaction in molten hydrocarbon for Li-ion battery cathode. *Nano Lett.* **2010**, *10*, 2799–2805. [CrossRef] [PubMed]
72. Bakenov, Z.; Taniguchi, I. Electrochemical performance of nanocomposite $LiMnPO_4$/C cathode materials for lithium batteries. *Electrochem. Commun.* **2010**, *12*, 75–78. [CrossRef]

73. Yoshida, J.; Stark, M.; Holzbock, J.; Hüsing, N.; Nakanishi, S.; Iba, H.; Abe, H.; Naito, M. Analysis of the size effect of $LiMnPO_4$ particles on the battery properties by using STEM-EELS. *J. Power Sources* **2013**, *226*, 122–126. [CrossRef]
74. Taniguchi, I.; Doan, T.N.L.; Shao, B. Synthesis and electrochemical characterization of $LiCo_xMn_{1-x}PO_4/C$ nanocomposites. *Electrochim. Acta* **2011**, *56*, 7680–7685. [CrossRef]
75. Ji, H.; Yang, G.; Ni, H.; Roy, S.; Pinto, J.; Jiang, X. General synthesis and morphology control of $LiMnPO_4$ nanocrystals via microwave-hydrothermal route. *Electrochim. Acta* **2011**, *56*, 3093–3100. [CrossRef]
76. Sheem, K.; Lee, Y.H.; Lim, H.S. High-density positive electrodes containing carbon nanotubes for use in Li-ion cells. *J. Power Sources* **2006**, *158*, 1425–1430. [CrossRef]
77. Wang, L.; Huang, Y.; Jiang, R.; Jia, D. Nano-$LiFePO_4$/MWCNT Cathode Materials Prepared by Room-Temperature Solid-State Reaction and Microwave Heating. *J. Electrochem. Soc.* **2007**, *154*, A1015–A1019. [CrossRef]
78. Liu, X.-M.; Huang, Z.-D.; Oh, S.; Ma, P.-C.; Chan, P.C.H.; Vedam, G.K.; Kang, K.; Kim, J.-K. Sol–gel synthesis of multiwalled carbon nanotube-$LiMn_2O_4$ nanocomposites as cathode materials for Li-ion batteries. *J. Power Sources* **2010**, *195*, 4290–4296. [CrossRef]
79. Varzi, A.; Bresser, D.; Zamory, J.V.; Müller, F.; Passerini, S. $ZnFe_2O_4$-C/$LiFePO_4$-CNT: A Novel High-Power Lithium-Ion Battery with Excellent Cycling Performance. *Adv. Energy Mater.* **2014**, *4*, 1400054–1400062. [CrossRef] [PubMed]
80. Schneider, J.J.; Khanderi, J.; Popp, A.; Engstler, J.; Tempel, H.; Sarapulova, A.; Bramnik, N.N.; Mikhailova, D.; Ehrenberg, H.; Schmitt, L.A.; et al. Hybrid Architectures from 3D Aligned Arrays of Multiwall Carbon Nanotubes and Nanoparticulate $LiCoPO_4$: Synthesis, Properties and Evaluation of Their Electrochemical Performance as Cathode Materials in Lithium Ion Batteries. *Eur. J. Inorg. Chem.* **2011**, 4349–4359. [CrossRef]
81. Dettlaff-Weglikowska, U.; Yoshida, J.; Sato, N.; Roth, S. Single walled carbon nanotubes for efficient electronic and ionic transport in the lithium ion batteries. *ECS Trans.* **2010**, *25*, 211–217. [CrossRef]
82. Geim, A.K. Graphene:Status and Prospects. *Science* **2009**, *324*, 1530–1534. [CrossRef] [PubMed]
83. Geim, A.K.; Novoselov, K.S. The rise of graphene. *Nat. Mater.* **2007**, *6*, 183–191. [CrossRef] [PubMed]
84. Lee, C.; Wei, X.; Kysar, J.W.; Hone, J. Measurement of the Elastic Properties and Intrinsic Strength of Monolayer Graphene. *Science* **2008**, *321*, 385–388. [CrossRef] [PubMed]
85. Park, S.; Ruoff, R.S. Chemical methods for the production of graphenes. *Nat. Nanotechnol.* **2009**, *4*, 217–224. [CrossRef] [PubMed]
86. Varzi, A.; Täubert, C.; Wohlfahrt-Mehrens, M.; Kreis, M.; Schütz, W. Study of multi-walled carbon nanotubes for lithium-ion battery electrodes. *J. Power Sources* **2011**, *196*, 3303–3309. [CrossRef]
87. Murugan, A.V.; Muraliganth, T.; Ferreira, P.J.; Manthiram, A. Dimensionally Modulated, Single-Crystalline $LiMPO_4$ (M = Mn, Fe, Co, and Ni) with Nano-Thumblike Shapes for High-Power Energy Storage. *Inorg. Chem.* **2009**, *48*, 946–952. [CrossRef] [PubMed]
88. Kavan, L.; Bacsa, R.; Tunckol, M.; Serp, P.; Zakeeruddin, S.M.; Formal, F.L.; Zukalova, M.; Graetzel, M. Multi-walled carbon nanotubes functionalized by carboxylic groups: Activation of TiO_2 (anatase) and phosphate olivines ($LiMnPO_4$; $LiFePO_4$) for electrochemical Li-storage. *J. Power Sources* **2010**, *195*, 5360–5369. [CrossRef]
89. Kucinskis, G.; Bajars, G.; Kleperis, J. Graphene in lithium ion battery cathode materials: A review. *J. Power Sources* **2013**, *240*, 66–79. [CrossRef]
90. Raccichini, R.; Varzi, A.; Passerini, S.; Scrosati, B. The role of graphene for electrochemical energy storage. *Nat. Mater.* **2015**, *14*, 271–279. [CrossRef] [PubMed]
91. Wang, H.; Yang, Y.; Liang, Y.; Cui, L.-F.; Casalongue, H.; Li, Y.; Hong, G.; Cui, Y.; Dai, H. $LiMn_{1-x}Fe_xPO_4$ nanorods grown on graphene sheets for ultrahigh-rate-performance lithium ion batteries. *Angew. Chem.* **2011**, *50*, 7364–7368. [CrossRef] [PubMed]
92. Qin, Z.; Zhou, X.; Xia, Y.; Tang, C.; Liu, Z. Morphology controlled synthesis and modification of high-performance $LiMnPO_4$ cathode materials for Li-ion batteries. *J. Mater. Chem.* **2012**, *22*, 21144–21153. [CrossRef]
93. Jiang, Y.; Liu, R.; Xu, W.; Jiao, Z.; Wu, M.; Chu, Y.; Su, L.; Cao, H.; Hou, M.; Zhao, B. A novel graphene modified $LiMnPO_4$ as a performance-improved cathode material for lithium-ion batteries. *J. Mater. Res.* **2013**, *28*, 2584–2589. [CrossRef]
94. Hummers, W.S.; Offeman, R.E. Preparation of Graphitic Oxide. *J. Am. Chem. Soc.* **1958**, *80*, 1339. [CrossRef]

95. Su, F.-Y.; He, Y.-B.; Li, B.; Chen, X.-C.; You, C.-H.; Wei, W.; Lv, W.; Yang, Q.-H.; Kang, F. Could graphene construct an effective conducting network in a high-power lithium ion battery? *Nano Energy* **2012**, *1*, 429–439. [CrossRef]
96. Zhang, W.; Zeng, Y.; Xu, C.; Xiao, N.; Gao, Y.; Li, L.J.; Chen, X.; Hng, H.H.; Yan, Q. A facile approach to nanoarchitectured three-dimensional graphene-based Li-Mn-O composite as high-power cathodes for Li-ion batteries. *Beilstein J. Nanotechnol.* **2012**, *3*, 513–523. [CrossRef] [PubMed]
97. Su, F.-Y.; You, C.; He, Y.-B.; Lv, W.; Cui, W.; Jin, F.; Li, B.; Yang, Q.-H.; Kang, F. Flexible and planar graphene conductive additives for lithium-ion batteries. *J. Mater. Chem.* **2010**, *20*, 9644–9650. [CrossRef]
98. Yadav, T.P.; Tiwari, R.S.; Srivastava, O.N.; Mukhopadhyay, N.K. Evolution of a Nanocrystalline (Co,Ni)Al_2O_4 Spinel Phase from Quasicrystalline Precursor. *Int. J. Appl. Ceram. Technol.* **2008**, *5*, 449–457. [CrossRef]
99. Franger, S.; Le Cras, F.; Bourbon, C.; Rouault, H. Comparison between different $LiFePO_4$ synthesis routes and their influence on its physico-chemical properties. *J. Power Sources* **2003**, *119*, 252–257. [CrossRef]
100. Kwon, S.J.; Kim, C.W.; Jeong, W.T.; Lee, K.S. Synthesis and electrochemical properties of olivine $LiFePO_4$ as a cathode material prepared by mechanical alloying. *J. Power Sources* **2004**, *137*, 93–99. [CrossRef]
101. Shin, H.C.; Cho, W.I.; Jang, H. Electrochemical properties of carbon-coated $LiFePO_4$ cathode using graphite, carbon black, and acetylene black. *Electrochim. Acta* **2006**, *52*, 1472–1476. [CrossRef]
102. Hong, S.-H.; Kim, B.-K. Fabrication of W–20 wt % Cu composite nanopowder and sintered alloy with high thermal conductivity. *Mater. Lett.* **2003**, *57*, 2761–2767. [CrossRef]
103. Guerfi, A.; Sévigny, S.; Lagacé, M.; Hovington, P.; Kinoshita, K.; Zaghib, K. Nano-particle $Li_4Ti_5O_{12}$ spinel as electrode for electrochemical generators. *J. Power Sources* **2003**, *119–121*, 88–94. [CrossRef]
104. Kim, B.K.; Ha, G.H.; Lee, G.G.; Lee, D.W. Structure and properties of nanophase WC/Co/VC/TaC hardmetal. *Nanostruct. Mater.* **1997**, *9*, 233–236. [CrossRef]
105. Xing, T.; Sunarso, J.; Yang, W.; Yin, Y.; Glushenkov, A.M.; Li, L.H.; Howlett, P.C.; Chen, Y. Ball milling: A green mechanochemical approach for synthesis of nitrogen doped carbon nanoparticles. *Nanoscale* **2013**, *5*, 7970–7976. [CrossRef] [PubMed]
106. Scholz, G.; König, R.; Petersen, J.; Angelow, B.; Dörfel, I.; Kemnitz, E. Mechanical Activation of α-AlF_3:Changes in Structure and Reactivity. *Chem. Mater.* **2008**, *20*, 5406–5413. [CrossRef]
107. Zheng, Z.G.; Zhong, X.C.; Zhang, Y.H.; Yu, H.Y.; Zeng, D.C. Synthesis, structure and magnetic properties of nanocrystalline $Zn_xMn_{1-x}Fe_2O_4$ prepared by ball milling. *J. Alloy. Compd.* **2008**, *466*, 377–382. [CrossRef]
108. Yadav, T.P.; Yadav, R.M.; Singh, D.P. Mechanical Milling: A Top Down Approach for the Synthesis of Nanomaterials and Nanocomposites. *J. Nanosci. Nanotechnol.* **2012**, *2*, 22–48. [CrossRef]
109. Suryanarayana, C. *Bibliography on Mechanical Alloying and Milling*; Cambridge Interscience Publisher: Cambridge, UK, 1995.
110. Ong, T.S.; Yang, H. Effect of atmosphere on the mechanical milling of natural graphite. *Carbon* **2000**, *38*, 2077–2085. [CrossRef]
111. Chen, Y.; Fitz Gerald, J.; Chadderton, L.T.; Chaffron, L. Nanoporous carbon produced by ball milling. *Appl. Phys. Lett.* **1999**, *74*, 2782–2784. [CrossRef]
112. Tarascon, J.M.; Morcrette, M.; Saint, J.; Aymard, L.; Janot, R. On the benefits of ball milling within the field of rechargeable Li-based batteries. *C. R. Chim.* **2005**, *8*, 17–26. [CrossRef]
113. Weeber, A.W.; Bakker, H. Amorphization by ball milling. A review. *Phs. B Condens. Matter* **1988**, *153*, 93–135. [CrossRef]
114. Michel, D.; Mazerolles, L.; Gaffet, E. Nanocrystalline oxide powders prepared by ball-milling. *Third Euro-Ceram.* **1993**, *1*, 255–260.
115. Welham, N.J.; Berbenni, V.; Chapman, P.G. Effect of extended ball milling on graphite. *J. Alloy. Compd.* **2003**, *349*, 255–263. [CrossRef]
116. Welham, N.J.; Williams, J.S. Extended milling of graphite and activated carbon. *Carbon* **1998**, *36*, 1309–1315. [CrossRef]
117. Liu, F.; Zhang, X.; Cheng, J.; Tu, J.; Kong, F.; Huang, W.; Chen, C. Preparation of short carbon nanotubes by mechanical ball milling and their hydrogen adsorption behavior. *Carbon* **2003**, *41*, 2527–2532. [CrossRef]
118. Kwon, N.H.; Brog, J.P.; Maharajan, S.; Crochet, A.; Fromm, K.M. Nanomaterials Meet Li-ion Batteries. *Chimia* **2015**, *69*, 734–736. [CrossRef] [PubMed]
119. Mouck-Makanda, D. *High-Energy Olivine Structured Cathodes for Li-Ion Batteries*; Université de Fribourg: Fribourg, Switzerland; Université du Maine: Le Mans, France, 2016.

120. Pierard, N.; Fonseca, A.; Colomer, J.F.; Bossuot, C.; Benoit, J.M.; Van Tendeloo, G.; Pirard, J.P.; Nagy, J.B. Ball milling effect on the structure of single-wall carbon nanotubes. *Carbon* **2004**, *42*, 1691–1697. [CrossRef]
121. Gao, B.; Bower, C.; Lorentzen, J.D.; Fleming, L.; Kleinhammes, A.; Tang, X.P.; McNeil, L.E.; Wu, Y.; Zhou, O. Enhanced saturation lithium composition in ball-milled single-walled carbon nanotubes. *Chem. Phys. Lett.* **2000**, *327*, 69–75. [CrossRef]
122. Ahn, J.H.; Shin, H.S.; Kim, Y.J.; Chung, H. Structural modification of carbon nanotubes by various ball milling. *J. Alloy. Compd.* **2007**, *434–435*, 428–432. [CrossRef]
123. Wang, Y.; Deng, W.; Liu, X.; Wang, X. Electrochemical hydrogen storage properties of ball-milled multi-wall carbon nanotubes. *Int. J. Hydrogen Energy* **2009**, *34*, 1437–1443. [CrossRef]
124. Lyu, H.; Gao, B.; He, F.; Ding, C.; Tang, J.; Crittenden, J.C. Ball-Milled Carbon Nanomaterials for Energy and Environmental Applications. *ACS Sustain. Chem. Eng.* **2017**, *5*, 9568–9585. [CrossRef]
125. Xu, J.; Thomas, H.R.; Francis, R.W.; Lum, K.R.; Wang, J.; Liang, B. A review of processes and technologies for the recycling of lithium-ion secondary batteries. *J. Power Sources* **2008**, *177*, 512–527. [CrossRef]
126. Zheng, H.; Yang, R.; Liu, G.; Song, X.; Battaglia, V.S. Cooperation between Active Material, Polymeric Binder and Conductive Carbon Additive in Lithium Ion Battery Cathode. *J. Phys. Chem. C* **2012**, *116*, 4875–4882. [CrossRef]
127. Martha, S.K.; Grinblat, J.; Haik, O.; Zinigrad, E.; Drezen, T.; Miners, J.H.; Exnar, I.; Kay, A.; Markovsky, B.; Aurbach, D. $LiMn_{0.8}Fe_{0.2}PO_4$: An Advanced Cathode Material for Rechargeable Lithium Batteries. *Angew. Chem.* **2009**, *48*, 8711–8715. [CrossRef] [PubMed]
128. Kwon, N.H. The effect of carbon morphology on the $LiCoO_2$ cathode of lithium ion batteries. *Solid State Sci.* **2013**, *21*, 59–65. [CrossRef]
129. Luo, S.; Wang, K.; Wang, J.; Jiang, K.; Li, Q.; Fan, S. Binder-Free $LiCoO_2$/Carbon Nanotube Cathodes for High-Performance Lithium Ion Batteries. *Adv. Mater.* **2012**, *24*, 2294–2298. [CrossRef] [PubMed]
130. Jo, M.; Jeong, S.; Cho, J. High power $LiCoO_2$ cathode materials with ultra energy density for Li-ion cells. *Electrochem. Commun.* **2010**, *12*, 992–995. [CrossRef]
131. Burukhin, A.; Brylev, O.; Hany, P.; Churagulov, B.R. Hydrothermal synthesis of $LiCoO_2$ for lithium rechargeable batteries. *Solid State Ion.* **2002**, *151*, 259–263. [CrossRef]
132. Wang, H.; Jang, Y.-I.; Huang, B.; Sadowa, D.R.; Chiang, Y.M. TEM Study of Electrochemical Cycling-Induced Damage and Disorder in $LiCoO_2$ Cathodes for Rechargeable Lithium Batteries. *J. Electrochem. Soc.* **1999**, *146*, 473–480. [CrossRef]
133. Yazami, R.; Lebrun, N.; Bonneau, M.; Molteni, M. High-Performance $LiCoO_2$ Positive Electrode Material. *J. Power Sources* **1995**, *54*, 389–392. [CrossRef]
134. Kwon, N.H.; Yin, H.; Brodard, P.; Sugnaux, C.; Fromm, K.M. Impact of composite structure and morphology on electronic and ionic conductivity of carbon contained $LiCoO_2$ cathode. *Elecrochim. Acta* **2014**, *134*, 215–221. [CrossRef]
135. Uno, Y.; Tachimori, K.; Tsujikawa, T.; Hirai, T. Effect of carbon coating on electrochemical properties of $LiCoO_2$-Nanocarbon composites. *ECS Trans.* **2010**, *25*, 121–125. [CrossRef]
136. Nemanich, R.J.; Solin, S.A. First- and second-order Raman scattering from finite-size crystals of graphite. *Phys. Rev. B* **1979**, *20*, 392–401. [CrossRef]
137. Ferrari, A.C.; Robertson, J. Interpretation of Raman spectra of disordered and amorphous carbon. *Phys. Rev. B* **2000**, *61*, 14095–14107. [CrossRef]
138. Kinoshita, K. *Chemical and Surface Properties*; John Wiley & Sons, Inc.: Hoboken, NJ, USA, 1988.
139. Pimenta, M.A.; Dresselhaus, G.; Dresselhaus, M.S.; Canado, L.G.; Jorio, A.; Saito, R. Studying disorder in graphite-based systems by Raman spectroscopy. *Phys. Chem. Chem. Phys.* **2007**, *9*, 1276–1291. [CrossRef] [PubMed]
140. Shen, T.D.; Ge, W.Q.; Wang, K.Y.; Quan, M.X.; Wang, J.T.; Wei, W.D.; Koch, C.C. Structural disorder and phase transformation in graphite produced by ball miling. *Nanostruct. Mater.* **1996**, *7*, 393–399. [CrossRef]